On stable, dissipation reducing splitting schemes for two-phase flow of electrolyte solutions

Stefan Metzger

Numerical Algorithms

ISSN 1017-1398

Numer Algor
DOI 10.1007/s11075-018-0530-2

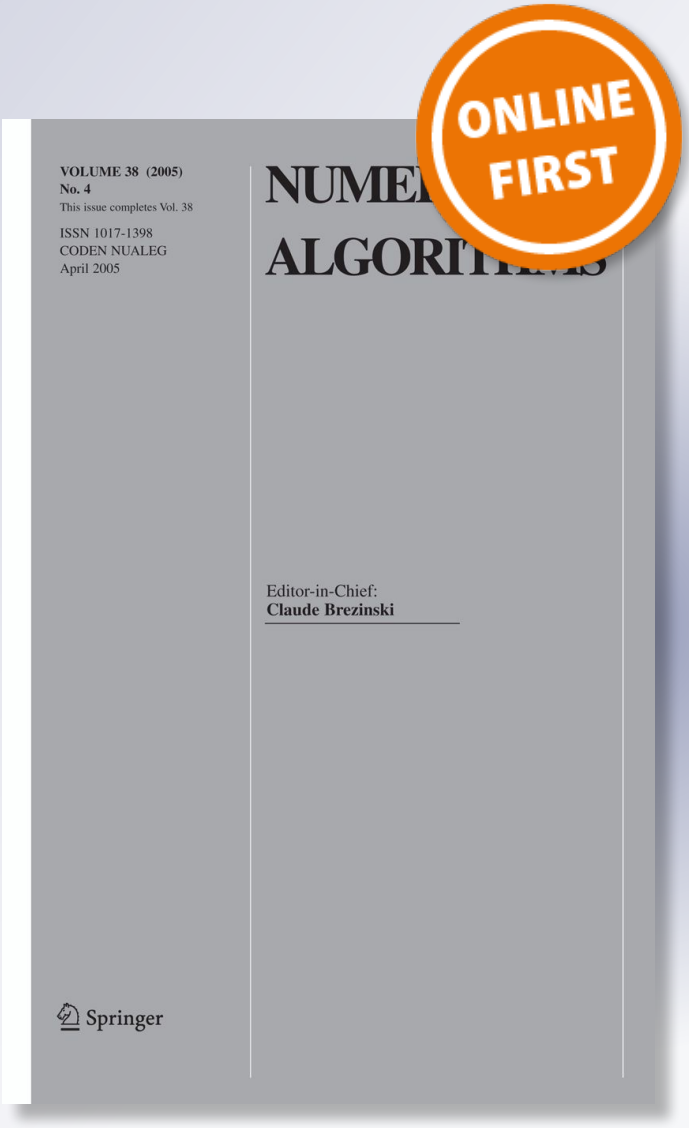

Springer

Numer Algor
https://doi.org/10.1007/s11075-018-0530-2

ORIGINAL PAPER

On stable, dissipation reducing splitting schemes for two-phase flow of electrolyte solutions

Stefan Metzger[1]

Received: 22 August 2017 / Accepted: 9 April 2018

Abstract In this paper, we are concerned with the numerical treatment of a recent diffuse interface model for two-phase flow of electrolyte solutions (Campillo-Funollet et al., SIAM J. Appl. Math. **72**(6), 1899–1925, 2012) . This model consists of a Nernst–Planck-system describing the evolution of the ion densities and the electrostatic potential which is coupled to a Cahn–Hilliard–Navier–Stokes-system describing the evolution of phase-field, velocity field, and pressure. In the first part, we present a stable, fully discrete splitting scheme, which allows to split the governing equations into different blocks, which may be treated sequentially and thereby reduces the computational costs significantly. This scheme comprises different mechanisms to reduce the induced numerical dissipation. In the second part, we investigate the impact of these mechanisms on the scheme's sensitivity to the size of the time increment using the example of a falling droplet. Finally, we shall present simulations showing ion induced changes in the topology of charged droplets serving as a qualitative validation for our discretization and the underlying model.

Keywords Electrolyte solutions · Phase-field model · Navier–Stokes equations · Cahn–Hilliard equation · Nernst–Planck equations · Finite element scheme · Splitting scheme

Mathematics Subject Classification (2010) 35Q35 · 65M60 · 65M12 · 76D05 · 76T99 · 76W05

✉ Stefan Metzger
stefan.metzger@fau.de

[1] Department Mathematik, Friedrich-Alexander-Universität Erlangen-Nürnberg, Cauerstr. 11, 91058 Erlangen, Germany

Published online: 23 April 2018

1 Introduction

In this paper, we are concerned with the numerical treatment of a diffuse interface model for two-phase flow of electrolyte solutions (cf. [5]) The model describes the evolution of two immiscible fluids with several dissolved species differing in valence and solubility properties. It is based on a diffuse interface description with a solenoidal, volume-averaged velocity field u (cf. [1]), and reads as follows.

$$\partial_t(\rho(\phi)u) + \operatorname{div}\{\rho(\phi)u\otimes u\} - \operatorname{div}\left\{u\otimes \rho'(\phi)m(\phi)\nabla\mu_\phi\right\} - \operatorname{div}\{2\eta(\phi)Du\} + \nabla p = \mu_\phi\nabla\phi + \sum_{j=1}^{K}\mu_{\omega_j}\nabla\omega_j - \sum_{j=1}^{K} z_j\omega_j\nabla V\,, \tag{1.1a}$$

$$\operatorname{div} u = 0\,, \tag{1.1b}$$

$$\partial_t\phi + u\cdot\nabla\phi - \operatorname{div}\left\{m(\phi)\nabla\mu_\phi\right\} = 0\,, \tag{1.1c}$$

$$\mu_\phi = \frac{\partial f(\phi,\nabla\phi)}{\partial\phi} - \operatorname{div}\left\{\frac{\partial f(\phi,\nabla\phi)}{\partial\nabla\phi}\right\} + \sum_{j=1}^{K}\beta_j'(\phi)\omega_j - \tfrac{1}{2}\partial_\phi\epsilon\,|\nabla V|\,, \tag{1.1d}$$

$$\partial_t\omega_i + u\cdot\nabla\omega_i - \operatorname{div}\left\{k(\phi)\omega_i\nabla(\mu_{\omega_i} + z_iV)\right\} = R_i\,, \tag{1.1e}$$

$$\mu_{\omega_i} = g'(\omega_i) + \beta_i(\phi) \qquad (i = 1,\ldots,K) \tag{1.1f}$$

on $\Omega\times\mathbb{R}^+$, together with

$$-\operatorname{div}\{\epsilon[\phi]\nabla V\} = \sum_{j=1}^{K} z_j\omega_j\chi_\Omega \tag{1.1g}$$

on $\Omega^*\times\mathbb{R}^+$, completed with the boundary conditions

$$u = 0\,,\quad m(\phi)\nabla\mu_\phi\cdot n = 0\,,\quad k(\phi)\omega_i\nabla(\mu_{\omega_i}+z_iV)\cdot n = 0 \quad \text{on } \partial\Omega\times\mathbb{R}^+\,, \tag{1.1h}$$

$$\frac{\partial f}{\partial\nabla\phi}\cdot n = -\alpha\partial_t\phi - \gamma_{fs}'(\phi) \qquad \text{on } \partial\Omega\times\mathbb{R}^+\,, \tag{1.1i}$$

$$V = \overline{V} \qquad \text{on } \partial\Omega^*\times\mathbb{R}^+\,. \tag{1.1j}$$

The (1.1a)–(1.1d) represent the phase-field description of the balance of mass (depending linearly on the phase-field parameter ϕ via $\rho(\phi) = \frac{1}{2}(\tilde\rho_2+\tilde\rho_1) + \frac{1}{2}(\tilde\rho_2-\tilde\rho_1)\phi$ with $\tilde\rho_1$ and $\tilde\rho_2$ denoting the mass densities of the pure phases) and momentum of two immiscible fluids which are confined to the domain $\Omega\subset\mathbb{R}^d$, $d = 2$ or 3. Thereby, m is the mobility. The Nernst–Planck-system (1.1e)–(1.1g) describes the evolution of the electrostatic potential V and of the number densities $\{\omega_i\}_{i=1,\ldots,K}$ of the K dissolved species having valence z_i $(i = 1,..,K)$ and individual solubility properties described by a solubility energy of the form $\int_\Omega\beta_i(\phi)\omega_i$ $(i = 1,\ldots,K)$. Thereby, the electrostatic potential V is considered on a larger domain $\Omega^*\supset\Omega$ (cf. Fig. 1) to reduce the bias caused by the finite domain. Assuming

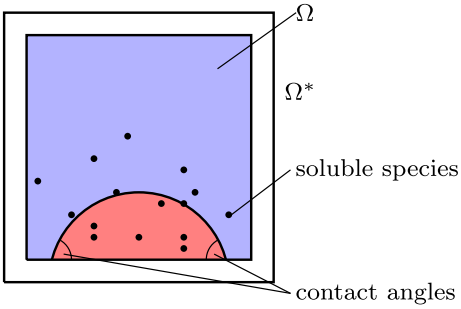

Fig. 1 Fluidic domain $\Omega \subset \Omega^*$ containing two fluids and soluble species

relatively small movements of electric charges, which do not create a substantial magnetic field, magnetic effects are neglected and the electric field equals the negative gradient of the electrostatic potential V.

While k_i are nonnegative coefficient functions depending solely on the fluids, the positive dielectric permittivity ϵ is also x-dependent, i.e., it depends on the fluids inside of Ω, but may also vary between Ω and $\Omega^* \backslash \Omega$. In particular, we use the notation

$$\epsilon[\phi](x) := \begin{cases} \tilde{\epsilon}(\phi(x)) & \text{if } x \in \overline{\Omega}, \\ \epsilon^*(x) & \text{if } x \in \overline{\Omega^*} \backslash \overline{\Omega} \end{cases} \tag{1.2}$$

with a fluid dependent permittivity $\tilde{\epsilon} : \mathbb{R} \to \mathbb{R}^+$ and a space dependent permittivity function $\epsilon^* : \overline{\Omega^*} \backslash \overline{\Omega} \to \mathbb{R}^+$.
Formal computations show that an energy of form

$$\begin{aligned} \mathcal{E}(\phi, \{\omega_i\}_{i=1,\dots,K}, V, u) := & \int_\Omega f(\phi, \nabla\phi) + \int_{\partial\Omega} \gamma_{fs}(\phi) + \sum_{i=1}^{K} \int_\Omega g(\omega_i) \\ & + \sum_{i=1}^{K} \int_\Omega \beta_i(\phi)\omega_i + \int_{\Omega^*} \epsilon[\phi](x)\, |\nabla V|^2 \\ & + \int_\Omega \tfrac{1}{2}\rho\, |u|^2 \,, \end{aligned} \tag{1.3}$$

acts as a Lyapunov functional (cf. [5]). Thereby, the Cahn–Hilliard free energy $\int_\Omega f(\phi, \nabla\phi)$ describes the fluid-fluid contact energy, while the second component models the fluid-solid contact energy with some ϕ-dependent energy density γ_{fs}. The next two ingredients describe the contributions of the species. In particular, there is an entropic component $\int_\Omega g(\omega_i)$ with $g(s) := s \log s - s$ and the solubility energy $\int_\Omega \beta_i(\phi)\omega_i$ for each species. The last two terms in (1.3) describe the contribution of the electrostatic potential and the kinetic energy.
Throughout this paper, we assume the Cahn–Hilliard free energy density to be of the form $f(\phi, \nabla\phi) := \frac{\sigma\delta}{2} |\nabla\phi|^2 + \frac{\sigma}{\delta} W(\phi)$, where the parameter σ corresponds to the surface tension, the parameter δ describes the width of the diffuse interface, and W is double-well potential with minima in ± 1. In this case, boundary condition (1.1i) reads

$$\delta\sigma \nabla\phi \cdot n = -\alpha \partial_t \phi - \gamma'_{fs}(\phi) \,. \tag{1.3}$$

The meaning of this boundary condition was elucidated of [17] (with reference to [22]). For $\alpha = 0$, Young's formula for the contact angle between the wall and the moving interface may be recovered. For an application of this boundary condition, we refer to [2], where a suitable choice of γ_{fs} was successfully used to prevent a rising bubble from sticking to the wall of a narrow channel. The choice $\alpha > 0$ allows for contact angle hysteresis (cf. [5, 22]), i.e., the advancing contact angle is larger than the static contact angle, and the latter is larger than the receding contact angle.

In the original model in [5], the electrostatic potential V is subjected to Dirichlet boundary conditions on $\partial\Omega^*$. Nevertheless, it was already suggested in Section 7.2.4 of that publication to consider Dirichlet boundary data only on a nonempty subset Γ_D of $\partial\Omega^*$ and to impose homogeneous Neumann boundary conditions on $\partial\Omega^* \setminus \Gamma_D$. As expatiated in [17], the Dirichlet boundary mimics a (maybe grounded) electrode, whereas the Neumann boundary is chosen to reduce the bias caused by considering the electric field only on a finite domain. With this in mind, we replace (1.1j) by

$$V = \overline{V} \qquad \text{on } \Gamma_D \times \mathbb{R}^+, \tag{1.5a}$$

$$\nabla V \cdot n = 0 \qquad \text{on } (\partial\Omega^* \setminus \Gamma_D) \times \mathbb{R}^+. \tag{1.5b}$$

The reaction terms R_i in (1.1e) are suggested to obey a generalization of the law of mass action. Namely, they may be written as

$$R_i(\{\mu_{\omega_j}\}_{j=1,\dots,K}, V) := \zeta_i \left[\exp\left(\sum_{\zeta_j < 0} |\zeta_j| \left(\mu_{\omega_j} + z_j V\right) \right) - \exp\left(\sum_{\zeta_j \geq 0} \zeta_j \left(\mu_{\omega_j} + z_j V\right) \right) \right]. \tag{1.6}$$

To simplify the notation, we suppressed the dependency of R_i on $\{\mu_{\omega_j}\}_{j=1,\dots,K}$ and V in (1.1a). The coefficients ζ_i $(i = 1, \dots, K)$ in (1.6) depend on the stoichiometric coefficients.

Other modeling approaches can be found, e.g. in [8] and [9]. The model investigated in the latter one also states evolution equations for different species which are coupled via reaction terms. However, it omits the energetic description of the solubility properties. Instead, degenerate coefficient functions were used to confine the species to one phase. The model presented in [8] also uses a degenerate coefficient function, but considers only one evolution equation for the charge density.

In Section 7 of [5], a simplified version of (1.1) was derived: Using a quadratic entropic functional instead of the logarithmic one linearizes the balance equations for the species concentrations and allows to combine them to one balance equation for the charge density. Omitting an energetic description of solubility properties, they confined the electric charges to one phase by introducing a suitable, degenerate coefficient function in the third term of (1.1e) (see also, e.g. [8]). First, numerical results for this simplified model based on finite element and finite volume approaches have already been published in [5]. A further investigation of discrete schemes for the aforementioned model was done in [17], where F. Klingbeil proved convergence of a finite element scheme for the case of homogeneous Dirichlet boundary conditions for the electrostatic potential.

A similar approach can also be found in [21], where the authors combined Cahn–Hilliard and Navier–Stokes type equations with a Nernst–Planck-system for the evolution of the charge density and the electric field. In [21], Nochetto et al. also proposed a coupled discrete scheme for the model and proved the stability of the scheme, as well as the existence of solutions. However, in order to perform simulations, the scheme was linearized with time-lagging of the variables.

In this paper, we propose a stable, fully discrete splitting scheme for (1.1). Splitting (1.1) into different blocks, which may be treated sequentially, allows to compute discrete solutions efficiently by omitting an iterative approach on the complete system. Similar splitting ideas have previously been used in [3, 20], and [15] for a model of magnetohydrodynamics and for diffuse interface models for multi-phase flows, respectively. In contrast to other splitting approaches—cf. [16], where a two-step scheme for Cahn–Hilliard–Navier–Stokes-systems was proposed—the presented schemes relies only on the data of the last time step. The presented scheme is an extension of the prototype suggested in [18]. In contrast to that prototype, the scheme presented in this publication omits the application of a cutoff function in the solubility energy and comprises different mechanisms to reduce the induced numerical dissipation, which are investigated by studying the example of a falling droplet.

The outline of the paper is as follows. In Section 2, we introduce the discrete function spaces and interpolation operators and state the discrete scheme. In Section 3, we establish the stability of the scheme for the general case of inhomogeneous Dirichlet boundary data $\overline{V}$ by proving that the discrete version of the energy is bounded from above by a positive constant which is independent of the discretization parameters. Based on this a priori estimate, we use Brouwer's fixed point theorem to show the existence of discrete solutions. A numerical investigation of the dissipation reducing mechanisms can be found in Section 4.1. Simulations serving as a qualitative validation of the presented scheme and the underlying model can be found in Sections 4.2 and 4.3.

The results presented in the following sections are excerpts from the author's Ph.D. thesis [19].

Notation To simplify the notation, we will assume that the mobility m and the coefficient functions k_i ($i = 1, ..., K$) are constant (w.l.o.g. $m \equiv 1, k_i \equiv 1$ for $i = 1, ..., K$) for the remainder of this paper. However, the presented results are valid as long as these functions are nonnegative. We also set $\delta = \sigma = 1$ to simplify the notation.

By "$\cdot$", we denote the Euclidean scalar product on $\mathbb{R}^d$. For a given domain $\Omega \subset \mathbb{R}^d$ with $d \in \{2, 3\}$, we denote the space of k-times weakly differentiable functions with weak derivatives in $L^p(\Omega)$ by $W^{k,p}(\Omega)$. The symbol $W_0^{k,p}(\Omega)$ stands for the closure of $C_0^\infty(\Omega)$ in $W^{k,p}(\Omega)$. For $p = 2$, we will denote $W^{k,2}(\Omega)$ by $H^k(\Omega)$ and $W_0^{k,2}(\Omega)$ by $H_0^k(\Omega)$. Corresponding spaces of vector- and matrix-valued functions are denoted in boldface. For a Banach space Y and a time interval I, the symbol $L^p(I; Y)$ stands for the parabolic space of L^p-integrable functions on I with values in Y. Sometimes, we write Ω_T for the space-time cylinder $\Omega \times (0, T)$. The discrete function spaces will be introduced in Section 2.

2 A stable discrete splitting scheme

In this section, we present a fully discrete finite element scheme. Concerning the discretization in space and time, we assume that

(T) the time interval $I := [0, T)$ is subdivided in intervals $I_k := [t_k, t_{k+1})$ with $t_{k+1} = t_k + \tau_k$ for time increments $\tau_k > 0$ and $k = 0, ..., N-1$ with $t_N = T$. For simplicity, we take $\tau_k \equiv \tau = \frac{T}{N}$ for $k = 0, ..., N-1$.

The triangulations $\mathcal{T}_h^*$ and $\mathcal{T}_h$ of Ω^* and Ω are supposed to satisfy the following assumptions.

(S1) Let $\left\{\mathcal{T}_h^*\right\}_{h>0}$ be a quasiuniform family (in the sense of [4]) of partitions of Ω^* into disjoint, open simplices κ, so that

$$\overline{\Omega^*} \equiv \bigcup_{\kappa \in \mathcal{T}_h^*} \overline{\kappa} \quad \text{with} \quad h := \max_{\kappa \in \mathcal{T}_h^*} \operatorname{diam}(\kappa).$$

(S2) Let $\{\mathcal{T}_h\}_{h>0}$ be a quasiuniform family of partitions of Ω into simplices with $\mathcal{T}_h \subset \mathcal{T}_h^*$, so that $\overline{\Omega} \equiv \bigcup_{\kappa \in \mathcal{T}_h} \overline{\kappa}$.

Furthermore, we assume that the electrodes are not arbitrarily close to the fluidic domain.

(S3) The non-empty subset Γ_D of $\partial\Omega^*$ has a certain h-independent distance to Ω, i.e., there is a constant $c_\Gamma > 0$ such that $\operatorname{dist}(\Gamma_D, \Omega) \geq c_\Gamma$.

We use the standard reference simplex $\tilde{\kappa}$ with vertices $\{\tilde{P}_i\}_{i=0,...,d}$, where $\tilde{P}_0$ is the origin and the $\tilde{P}_i$ are such that the jth component of $\tilde{P}_i$ is δ_{ij} for $i, j = 1, ..., d$. Furthermore, we denote the vertices of an element $\kappa \in \mathcal{T}_h^*$ by $\{P_{\kappa,i}\}_{i=0,...,d}$ and define $\mathbf{B}_\kappa \in \mathbb{R}^{d\times d}$ such that the mapping $\mathcal{B}_\kappa : \mathbb{R}^d \ni y \mapsto P_{\kappa,0} + \mathbf{B}_\kappa y$ maps the vertex $\tilde{P}_i$ to $P_{\kappa,i}$ $(i = 0, ..., d)$ and hence $\tilde{\kappa}$ to κ.

Concerning the discrete function spaces, we denote the space of continuous, piecewise linear finite element functions on $\mathcal{T}_h$ by U_h and the extension to $\mathcal{T}_h^*$ by U_h^*. By $U_{h,0}^*$, we denote the subspace of U_h^* containing functions which vanish on $\Gamma_D \subset \partial\Omega^*$. Pressure and velocity field are approximated with the lowest order Taylor–Hood elements, i.e. S_h is the subspace of U_h containing only functions with zero mean and the space of continuous, piecewise quadratic, vector-valued finite element functions on $\mathcal{T}_h$ is denoted by $\boldsymbol{W}_h$, while $\boldsymbol{W}_{h,\mathrm{div}}$ denotes the subspace of weakly solenoidal vector-fields. In particular, we have

$$S_h := \left\{\theta_h \in U_h \,:\, \int_\Omega \theta_h \, \mathrm{d}\mathbf{x} = 0\right\}, \tag{2.1}$$

$$\boldsymbol{W}_{h,\mathrm{div}} := \left\{w_h \in \boldsymbol{W}_h \,:\, \int_\Omega \operatorname{div} w_h \theta_h = 0 \;\; \forall \theta_h \in S_h\right\}. \tag{2.2}$$

To project continuous functions onto U_h^* or U_h, we use the nodal interpolation operator $\mathcal{I}_h$ from $C^0(\overline{\Omega^*})$ to U_h^* which is defined by

$$\mathcal{I}_h\{a\} := \sum_{i=1}^{\dim U_h^*} a(x_i)\chi_{h,i}\,, \tag{2.3}$$

where the functions $\{\chi_{h,i}\}_{i=1,\dots,\dim U_h^*}$ form a dual basis to the vertices $\{x_i\}_{i=1,\dots,\dim U_h^*}$ of $\mathcal{T}_h^*$, i.e. $\chi_{h,i}(x_j) = \delta_{ij}$ for $i, j = 1, \dots, \dim U_h^*$. In a slight misuse of notation, we will denote the interpolation operator from $C^0(\overline{\Omega})$ to U_h also by $\mathcal{I}_h$. The backward difference quotient in time is denoted by ∂_τ^-.

As we are not able to guarantee the nonnegativity of the discrete number densities of the species $\omega_{h,i}$ $(i = 1, \dots, K)$ in the discrete setting, we define a regularized version of the entropic functional g via

$$g_\nu(s) := \begin{cases} s\log s - s & \text{if } s \geq \nu\,, \\ \frac{s^2-\nu^2}{2\nu} + (\log\nu - 1)s & \text{if } s < \nu\,, \end{cases} \tag{2.4a}$$

$$g_\nu'(s) = \begin{cases} \log s & \text{if } s \geq \nu\,, \\ \frac{s}{\nu} + \log\nu - 1 & \text{if } s < \nu\,, \end{cases} \tag{2.4b}$$

$$g_\nu''(s) = \max\{\nu, s\}^{-1}\,, \tag{2.4c}$$

for all $s \in \mathbb{R}$ and some regularization parameter $\nu > 0$. Using the ideas from [14], we define for a given function $\theta_h \in U_h$ and a given element $\kappa \in \mathcal{T}_h$ a diagonal matrix $\hat{\Xi}_\nu[\theta_h]$ by

$$\left[\hat{\Xi}_\nu[\theta_h]\right]_{ii} = \begin{cases} \frac{\theta_h(P_{\kappa,i}) - \theta_h(P_{\kappa,0})}{g_\nu'(\theta_h(P_{\kappa,i})) - g_\nu'(\theta_h(P_{\kappa,0}))} & \text{if } \theta_h(P_{\kappa,i}) \neq \theta_h(P_{\kappa,0})\,, \\ \frac{1}{g_\nu''(\theta_h(P_{\kappa,0}))} & \text{if } \theta_h(P_{\kappa,i}) = \theta_h(P_{\kappa,0})\,, \end{cases}. \tag{2.5a}$$

Incorporating the affine mapping from $\tilde{\kappa}$ to κ, we define the matrix-valued operator $\Xi_\nu[.]$ via

$$\Xi_\nu[\theta_h]\big|_\kappa := \mathbf{B}_\kappa^{-T}\,\hat{\Xi}_\nu[\theta_h]\,\mathbf{B}_\kappa^T \tag{2.5b}$$

for $\theta_h \in U_h$. A straight forward computation shows that this operator satisfies

$$\Xi_\nu[\theta_h]\nabla\mathcal{I}_h\left\{g_\nu'(\theta_h)\right\} = \nabla\theta_h \tag{2.6}$$

on Ω with $\theta_h \in U_h$. To guarantee positivity of the mass density, we use the regularized mass density function $\overline{\rho}$ satisfying

$$\overline{\rho}(\phi)\big|_{(-\overline{\phi},+\overline{\phi})} = \tfrac{\tilde{\rho}_2+\tilde{\rho}_1}{2} - \tfrac{\tilde{\rho}_2-\tilde{\rho}_1}{2}\phi\,, \tag{2.7a}$$

$$\overline{\rho}(\phi)\big|_{(-\infty,-\overline{\phi}]} \equiv \text{const}\,, \quad \overline{\rho}(\phi)\big|_{[+\overline{\phi},+\infty)} \equiv \text{const}\,, \tag{2.7b}$$

with $\overline{\phi} > 1$ small enough. As the original mass density ρ depends affine linearly on the phase-field parameter, we introduce $\frac{\delta\overline{\rho}}{\delta\phi} := \frac{\tilde{\rho}_2-\tilde{\rho}_1}{2}$ as an approximation of $\overline{\rho}'$ (cf. [11]).

Concerning the double-well potential W, we make assumptions similar to the ones used in [12], i.e.,

(W1) $W \in C^1(\mathbb{R}; \mathbb{R}_0^+)$ with $\left|W(s)s^{-3}\right| \to \infty$ for $|s| \to \infty$ such that W' is piecewise C^1 and that its derivatives have at most quadratic growth for $|s| \to \infty$.

Considering different discrete approximations of W' denoted by $W_h' : \mathbb{R}^2 \to \mathbb{R}_0^+$, we assume the following conditions to hold true.

(W2) There is a positive constant C such that for all $a, b \in \mathbb{R}$

$$\left|W_h'(a,b)\right| \leq C\left(1 + |a|^3 + |b|^3\right).$$

(W3) $W_h'(a,b)(a-b) \geq W(a) - W(b)$ for all $a, b \in \mathbb{R}$.

(W4) $W_h'(a,a) = W'(a)$ for all $a \in \mathbb{R}$.

(W5) There is a positive constant C, such that for all $a, b, c \in \mathbb{R}$

$$\left|W_h'(a,b) - W_h'(b,c)\right| \leq C(a^2+b^2+c^2)(|a-b| + |b-c|).$$

For instance, these conditions hold true for a polynomial double-well potential $\frac{1}{4}(1-\phi^2)^2$ with W_h' based on a difference quotient (cf. [12]). For numerical schemes based on a logarithmic-type double-well potential, we refer to [7]. Moreover, we define the difference quotients on $\overline{\Omega}$

$$\beta_{i,DQ}'(a,b) := \begin{cases} \frac{\beta_i(a)-\beta_i(b)}{a-b} & \text{if } a \neq b, \\ \beta_i'(a) & \text{if } a = b, \end{cases} \quad \forall i \in \{1, ..., K\}, \tag{2.8}$$

$$\gamma_{fs,DQ}'(a,b) := \begin{cases} \frac{\gamma_{fs}(a)-\gamma_{fs}(b)}{a-b} & \text{if } a \neq b, \\ \gamma_{fs}'(a) & \text{if } a = b, \end{cases} \tag{2.9}$$

$$\epsilon_{DQ}'(a,b) := \begin{cases} \frac{\tilde{\epsilon}(a)-\tilde{\epsilon}(b)}{a-b} & \text{if } a \neq b, \\ \partial_\phi \tilde{\epsilon}(\phi)\big|_{\phi=a} & \text{if } a = b. \end{cases} \tag{2.10}$$

The last difference quotient can naturally be extended to $\overline{\Omega^*}$ via $\epsilon_{DQ}'(a,b) \equiv 0$ on $\overline{\Omega^*} \backslash \overline{\Omega}$.

Using the abbreviations $\overline{\rho}_h^n := \mathcal{I}_h\left\{\overline{\rho}(\phi_h^n)\right\}$, $\epsilon_h^n := \mathcal{I}_h\left\{\epsilon[\phi_h^n](x)\right\}$, and

$$R_{i,h}^n := R_{i,h}(\phi_h^n, (\omega_h^n)^K, V_h^n) := \mathcal{I}_h\left\{\zeta_i\left[\exp\left(\sum_{\zeta_j<0}|\zeta_j|\left(g_v'(\omega_{j,h}^n) + \beta_j(\phi_h^n) + z_j V_h^n\right)\right)\right.\right.$$
$$\left.\left. - \exp\left(\sum_{\zeta_j \geq 0}\zeta_j\left(g_v'(\omega_{j,h}^n) + \beta_j(\phi_h^n) + z_j V_h^n\right)\right)\right]\right\}, \tag{2.11}$$

we state the following discrete scheme. For better readability, we write $(\theta_h)^K \in (U_h)^K$ for the tuple $(\theta_{i,h})_{i=1,...,K}$ with $\theta_{i,h} \in U_h$ for $i = 1, ..., K$.

Given $(\phi_h^{n-1}, (\omega_h^{n-1})^K, u_h^{n-1}) \in U_h \times (U_h)^K \times \boldsymbol{W}_{h,\mathrm{div}}$, and $\overline{V}_h^n \in U_h^*$, which defines the Dirichlet data of the electrostatic potential, find $(\phi_h^n, \mu_{\phi,h}^n, (\omega_h^n)^K, V_h^n - \overline{V}_h^n, u_h^n) \in U_h \times U_h \times (U_h)^K \times U_{h,0}^* \times \boldsymbol{W}_{h,\mathrm{div}}$ such that

$$\int_\Omega \mathcal{I}_h\{\partial_\tau^- \phi_h^n \theta_h\} - \int_\Omega \phi_h^{n-1} u_h^{n-1} \cdot \nabla\theta_h + \tau \int_\Omega (\min \overline{\rho}_h^{n-1})^{-1} \left|\phi_h^{n-1}\right|^2 \nabla\mu_{\phi,h}^n \cdot \nabla\theta_h + \int_\Omega \nabla\mu_{\phi,h}^n \cdot \nabla\theta_h = 0 \quad \forall \theta_h \in U_h\,, \tag{2.12a}$$

$$\int_\Omega \mathcal{I}_h\left\{\mu_{\phi,h}^n \theta_h\right\} = \int_\Omega (\vartheta \nabla\phi_h^n + (1-\vartheta)\nabla\phi_h^{n-1}) \cdot \nabla\theta_h + \int_\Omega \mathcal{I}_h\left\{W_h'(\phi_h^n, \phi_h^{n-1})\theta_h\right\} + \int_{\partial\Omega} \mathcal{I}_h\left\{\gamma_{fs,DQ}'(\phi_h^n, \phi_h^{n-1})\theta_h\right\} + \alpha \int_{\partial\Omega} \mathcal{I}_h\{\partial_\tau^- \phi_h^n \theta_h\} + \int_\Omega \mathcal{I}_h\left\{\sum_{j=1}^K \beta_{j,DQ}'(\phi_h^n, \phi_h^{n-1})\omega_{j,h}^{n-1}\theta_h\right\} - \tfrac{1}{2}\int_\Omega \mathcal{I}_h\left\{\epsilon_{DQ}'(\phi_h^n, \phi_h^{n-1})\theta_h\right\} \left|\nabla V_h^n\right|^2 \quad \forall \theta_h \in U_h\,, \tag{2.12b}$$

$$\int_\Omega \mathcal{I}_h\{\partial_\tau^- \omega_{i,h}^n \theta_h\} - \int_\Omega \omega_{i,h}^{n-1} u_h^{n-1} \cdot \nabla\theta_h + \tau K \int_\Omega (\min \overline{\rho}_h^{n-1})^{-1} \left|\omega_{i,h}^{n-1}\right|^2 \nabla\mathcal{I}_h\left\{g_\nu'(\omega_{i,h}^n) + \beta_i(\phi_h^n) + z_i V_h^n\right\} \cdot \nabla\theta_h + \int_\Omega \left(\Xi_\nu[\omega_{i,h}^n]\nabla\mathcal{I}_h\left\{g_\nu'(\omega_{i,h}^n) + \beta_i(\phi_h^n) + z_i V_h^n\right\}\right) \cdot \nabla\theta_h = \int_\Omega \mathcal{I}_h\left\{R_{i,h}^n \theta_h\right\} \quad \forall \theta_h \in U_h\,, \tag{2.12c}$$

$$\int_{\Omega^*} \epsilon_h^n \nabla V_h^n \cdot \nabla\theta_h = \int_\Omega \mathcal{I}_h\left\{\sum_{j=1}^K z_j \omega_{j,h}^n \theta_h\right\} \quad \forall \theta_h \in U_{h,0}^*\,, \tag{2.12d}$$

$$\int_\Omega \tfrac{1}{2}\left(\overline{\rho}_h^n + \overline{\rho}_h^{n-1}\right)\partial_\tau^- u_h^n \cdot w_h + \tfrac{1}{2}\int_\Omega \partial_\tau^- \overline{\rho}_h^n u_h^{n-1} \cdot w_h + \tfrac{1}{2}\int_\Omega \overline{\rho}_h^n \left((\nabla u_h^n)^T \cdot w_h\right) \cdot u_h^{n-1} - \tfrac{1}{2}\int_\Omega \overline{\rho}_h^n \left((\nabla w_h)^T \cdot u_h^n\right) \cdot u_h^{n-1} + \tfrac{1}{2}\int_\Omega \tfrac{\delta\overline{\rho}}{\delta\phi}\left((\nabla u_h^n)^T \cdot w_h\right) \cdot \nabla\mu_{\phi,h}^n - \tfrac{1}{2}\int_\Omega \tfrac{\delta\overline{\rho}}{\delta\phi}\left((\nabla w_h)^T \cdot u_h^n\right) \cdot \nabla\mu_{\phi,h}^n + \int_\Omega 2\mathcal{I}_h\{\eta(\phi_h^n)\} Du_h^n : Dw_h = -\int_\Omega \phi_h^{n-1} \nabla\mu_{\phi,h}^n \cdot w_h - \sum_{j=1}^K \int_\Omega \omega_{j,h}^{n-1} \nabla\mathcal{I}_h\left\{g_\nu'(\omega_{j,h}^n) + \beta_j(\phi_h^n) + z_j V_h^n\right\} \cdot w_h \quad \forall w_h \in \boldsymbol{W}_{h,\mathrm{div}} \tag{2.12e}$$

with $\alpha \geq 0$ describing contact angle hysteresis and the parameter $\vartheta \in [0.5, 1]$, which allows to reduce the numerical dissipation (cf. Section 4.1).

Remark 2.1 As the (2.12a)-(2.12d) are independent of u_h^n, we may compute ϕ_h^n, $\mu_{\phi,h}^n$, $(\omega_h^n)^K$ and V_h^n before solving the saddle-point problem (2.12e). If the dielectric permittivity ϵ is independent of the fluids, the last integral in (2.12b) vanishes allowing us to split (2.12) into three blocks which may be treated sequentially: The phase-field equations (2.12a) and (2.12b), the Nernst–Planck-system (2.12c) and (2.12d), and the momentum equations (2.12e).
The application of $\Xi_v[.]$ allows to rewrite the fourth term in (2.12c) as

$$\int_\Omega \nabla \omega_{i,h}^n \cdot \nabla \theta_h + \int_\Omega \left(\Xi_v[\omega_{i,h}^n] \nabla \mathcal{I}_h \left\{ \beta_i(\phi_h^n) + z_i V_h^n \right\} \right) \cdot \nabla \theta_h \,. \tag{2.13}$$

As this is not required for the stability of the scheme, a further reduction of the computational costs may be achieved by replacing $\Xi_v[\omega_{i,h}^n]$ in (2.12c) by an explicit, nonnegative expression like $\mathcal{I}_h \left\{ \left(g_v''(\omega_{i,h}^{n-1}) \right)^{-1} \right\}$.
A convergence result for this splitting approach applied to pure two-phase flows with different mass densities, i.e., sole Navier–Stokes–Cahn–Hilliard-systems, can be found in [12].

Straight forward computations show that the phase-field parameter and the number densities of species which do not participate in any reaction are conserved, i.e.,

$$\int_\Omega \phi_h^n = \int_\Omega \phi_h^{n-1} \quad \text{and} \quad \int_\Omega \omega_{i,h}^n = \int_\Omega \omega_{i,h}^{n-1} \quad \text{for all } i \in \{1, \ldots, K\} \text{ satisfying } \zeta_i = 0. \tag{2.14}$$

Under the additional assumption $\sum_{i=1}^K \zeta_i z_i = 0$, i.e., the considered reaction conserves the total charge of the involved molecules, the overall charge of the fluids $\int_\Omega \sum_{i=1}^K \omega_{i,h}^n z_i$ is also conserved.

3 Stability and existence of discrete solutions

This section is devoted to the stability properties of the splitting scheme introduced in (2.12). We prove that—under appropriate assumptions which are listed below—the aforementioned splitting scheme is stable. Based on this a priori stability result, we establish the existence of discrete solutions.
To prove the stability of the scheme and the existence of discrete solutions, we make the following general assumptions.

- **(E1)** Ω^* and Ω are open, bounded, convex polygonal (or polyhedral), and the discretization in space and time satisfies (T), (S1), (S2), and (S3).
- **(E2)** Assumptions (W1)–(W5) apply to the double-well potential W and W_h'.
- **(E3)** $\beta, \eta \in C^\infty(\mathbb{R}) \cap W^{1,\infty}(\mathbb{R})$ satisfying $0 \leq \beta(s)$ and $\eta(s) \geq c > 0$ for all $s \in \mathbb{R}$.
- **(E4)** The liquid-solid interfacial energy is described by $\gamma_{fs} \in C^\infty(\mathbb{R}) \cap W^{1,\infty}(\mathbb{R})$.
- **(E5)** The dielectric permittivity is defined via (1.2). It is bounded from above and below by positive constants $\epsilon_{\min}$ and $\epsilon_{\max}$. $\tilde{\epsilon} \in C^1(\mathbb{R})$ is piecewise constant

in $\mathbb{R}\setminus(-2,2)$. For technical reasons, let $\left|\frac{1}{2}(\tilde{\epsilon}(1)-\tilde{\epsilon}(-1))\right| = \sup\left|\tilde{\epsilon}'\right|$ and $\tilde{\epsilon}(0) = \frac{1}{2}(\tilde{\epsilon}(-1)+\tilde{\epsilon}(1))$ (cf. [17]).

(E6) The Dirichlet data for the electrostatic potential is given by the trace of functions $\overline{V}_h \in U_h^*$, which are bounded in $H^1(0,T;H^1(\Omega^*))$ independently of h, τ, and ν.

(E7) Initial data $\phi_h^0 \in U_h$, $\omega_{i,h}^0 \in U_h$ $(i=1,\ldots,K)$, and $u_h^0 \in \boldsymbol{W}_{h,\mathrm{div}}$ is given such that

$$\int_\Omega \left|\nabla\phi_h^0\right|^2 + \int_\Omega \mathcal{I}_h\left\{W(\phi_h^0)\right\} + \int_\Omega \left|u_h^0\right|^2 + \sum_{i=1}^K \int_\Omega \left|\omega_{i,h}^0\right|^2 \leq C \tag{3.1}$$

with $C>0$ independent of h, τ, and ν and $\omega_{i,h}^0 \geq 0$ $(i=1,\ldots,K)$.

Furthermore, we define the initial electrostatic potential V_h^0 as the solution of

$$\int_{\Omega^*} \mathcal{I}_h\left\{\epsilon[\phi_h^0](x)\right\}\nabla V_h^0\cdot\nabla\theta_h = \int_\Omega \mathcal{I}_h\left\{\sum_{j=1}^K z_j\omega_{j,h}^0\theta_h\right\} \tag{3.2}$$

for all $\theta_h \in U_{h,0}^*$ under the constraint $V_h^0 = \overline{V}_h^0$ on Γ_D.
In order to prove the stability of (2.12) even for inhomogeneous Dirichlet data for the electrostatic potential, we introduce a cutoff function. Recalling assumption (S3), we define the set $\Omega_{c_\Gamma} := \{x\in\overline{\Omega^*} : \mathrm{dist}\,(x,\Gamma_D)\geq c_\Gamma\}$ and obtain the inclusions

$$\Omega \subset \Omega_{c_\Gamma} \subset \overline{\Omega^*}. \tag{3.3}$$

We continue by defining a weight function ς mapping $\overline{\Omega^*}$ on the interval $[0,1]$ via

$$\varsigma(x) := \begin{cases} 1 & \text{if } x\in\Omega_{c_\Gamma}, \\ c_\Gamma^{-1}\,\mathrm{dist}\,(x,\Gamma_D) & \text{if } x\in\overline{\Omega^*}\setminus\Omega_{c_\Gamma}. \end{cases} \tag{3.4}$$

Finally, we define a discrete cut-off function $\Pi_{c_\Gamma} : U_h^* \to U_{h,0}^*$ via

$$\Pi_{c_\Gamma}(A_h) := \mathcal{I}_h\{\varsigma A_h\} \quad \text{for all} A_h \in U_h^*. \tag{3.5}$$

Lemma 3.1 *Let the Assumptions (S1), (S2), and (S3) hold true. Furthermore, let ς and Π_{c_Γ} be defined according to (3.4) and (3.5). Then, ς is Lipschitz continuous with Lipschitz constant c_Γ^{-1} and for any $A_h \in U_h^*$ the following pointwise estimate holds true on $\overline{\Omega^*}$.*

$$\left|\nabla\Pi_{c_\Gamma}(A_h)\right| \leq C\Big[|\nabla A_h| + c_\Gamma^{-1}\,|A_h|\Big]. \tag{3.6}$$

Proof The Lipschitz continuity follows from

$$|\varsigma(x)-\varsigma(y)| \leq c_\Gamma^{-1}\,|\mathrm{dist}\,(x,\Gamma_D)-\mathrm{dist}\,(y,\Gamma_D)| \leq c_\Gamma^{-1}\,|x-y| \tag{3.7}$$

for $x,y\in\overline{\Omega^*}$.
As ς is Lipschitz continuous, the estimate (3.6) may be proven following the lines of [10], Lemma 2.3. For the readers convenience, we summarize the proof. In a

first step, we consider a simplex $\kappa \in \mathcal{T}_h^*$ with vertices $\{P_{\kappa,i}\}_{i=0,...,d}$ and establish an analogous estimate for directional derivatives along the edges starting at $P_{\kappa,0}$. Parameterizing the edge between $P_{\kappa,0}$ and $P_{\kappa,i}$ by

$$c_i(s) := P_{\kappa,0} + s\frac{P_{\kappa,i} - P_{\kappa,0}}{\operatorname{dist}(P_{\kappa,i}, P_{\kappa,0})} =: P_{\kappa,0} + sv_i \quad s \in [0, \operatorname{dist}(P_{\kappa,i}, P_{\kappa,0})], \tag{3.8}$$

and denoting the dual basis to the vertices $\{P_{\kappa,i}\}_{i=0,...,d}$ by $\{\chi_{h,i}\}_{i=0,...,d}$, we compute the directional derivative along v_i

$$\partial_{v_i} A_h\big|_{c_i(s)} = A_h(P_{\kappa,0})\nabla\chi_{h,0}(c_i(s)) \cdot v_i + A_h(P_{\kappa,i})\nabla\chi_{h,i}(c_i(s)) \cdot v_i \tag{3.9}$$

for any $A_h \in U_h^*$ and $i = 1, ..., d$. To simplify the notation, we introduce $\varsigma_i := \varsigma(P_{\kappa,i})$ and $A_{h,i} := A_h(P_{\kappa,i})$ for $i = 0, ..., d$. In this notation, the directional derivatives of $\Pi_{c_\Gamma}(A_h)$ satisfy

$$\begin{aligned}
&\left|\partial_{v_i}\Pi_{c_\Gamma}(A_h)\right| = \left|\varsigma_0 A_{h,0}\nabla\chi_{h,0} \cdot v_i - \varsigma_i A_{h,i}\nabla\chi_{h,i} \cdot v_i\right| \\
&\leq \left|(A_{h,i} - A_{h,0})\nabla\chi_{h,i} \cdot v_i\right| + \left|A_{h,0}\right|\left|(\varsigma_i - \varsigma_0)\nabla\chi_{h,i} \cdot v_i\right| \leq \left|\partial_{v_i} A_h\right| + c_\Gamma^{-1}\left|A_{h,0}\right| .
\end{aligned} \tag{3.10}$$

To generalize (3.10) to estimates for the gradient of $\Pi_{c_\Gamma}(A_h)$, we define the invertible matrix $T := (v_1, ..., v_d)$ to obtain

$$\nabla\Pi_{c_\Gamma}(A_h) \cdot T = \left(\partial_{v_1}\Pi_{c_\Gamma}(A_h), ..., \partial_{v_d}\Pi_{c_\Gamma}(A_h)\right), \tag{3.11}$$

and consequently

$$\left\|\nabla\Pi_{c_\Gamma}(A_h)\right\|_1 \leq \left\|\left(\partial_{v_1}\Pi_{c_\Gamma}(A_h), ..., \partial_{v_d}\Pi_{c_\Gamma}(A_h)\right)\right\|_1 \left\|T^{-1}\right\| , \tag{3.12}$$

$$\left\|\left(\partial_{v_1}\Pi_{c_\Gamma}(A_h), ..., \partial_{v_d}\Pi_{c_\Gamma}(A_h)\right)\right\|_1 \leq \left\|\nabla\Pi_{c_\Gamma}(A_h)\right\|_1 \|T\| , \tag{3.13}$$

where $\|.\|$ is the matrix norm induced by the l^1 vector norm $\|.\|_1$. Combining (3.10), (3.12), and (3.13) provides

$$\begin{aligned}
\left\|\nabla\Pi_{c_\Gamma}(A_h)\right\|_1 &\leq \left\|\left(\partial_{v_1} A_h, ..., \partial_{v_d} A_h\right)\right\|_1 \left\|T^{-1}\right\| + dc_\Gamma^{-1}\left|A_{h,0}\right|\left\|T^{-1}\right\| \\
&\leq \|T\|\left\|T^{-1}\right\|\|\nabla A_h\|_1 + dc_\Gamma^{-1}\left\|T^{-1}\right\|\left|A_{h,0}\right| .
\end{aligned} \tag{3.14}$$

Using the affine linearity of A_h on κ, we choose $x \in \kappa$ and derive

$$\left|A_{h,0}\right| = \left|A_h(x) + \nabla A_h \cdot (P_{\kappa,0} - x)\right| \leq |A_h(x)| + Ch\,\|\nabla A_h\|_1 \tag{3.15}$$

making (3.14) independent of $A_h(P_{\kappa,0})$. To complete the proof, it remains to show that there is a constant $C > 0$ independent of h such that $\|T\| + \left\|T^{-1}\right\| \leq C$.
We want to emphasize that T does not belong to some affine transformation, which is mapping the reference simplex to an arbitrary simplex $\kappa \in \mathcal{T}_h^*$, as its column vectors $\{v_i\}_{i=1,...,d}$ have length one. Instead, T can be seen as a part of a function mapping the reference simplex to a stretched version of a simplex $\kappa \in \mathcal{T}_h^*$ with d edges of length one. Due to standard estimates (see, e.g. Theorem 3.1.3. in [6]), the norm of T and T^{-1} is bounded independently of h. For further details, we refer to the proof of Lemma 2.3 in [10]. □

Lemma 3.2 *Let Assumptions (E1)-(E7) hold true. Under the assumption that a discrete solution* $(\phi_h^n, \mu_{\phi,h}^n, (\omega_h^n)^K, V_h^n, u_h^n)_{n\geq 1}$ *to* (2.12) *exists, this solution satisfies*

$$\begin{aligned}
&\int_\Omega |\nabla\phi_h^n|^2 + \int_\Omega \mathcal{I}_h\{W(\phi_h^n)\} + \int_{\partial\Omega} \mathcal{I}_h\{\gamma_{fs}(\phi_h^n)\} + \sum_{j=1}^K \int_\Omega \mathcal{I}_h\left\{g_\nu(\omega_{j,h}^n)\right\} + \sum_{j=1}^K \int_\Omega \mathcal{I}_h\left\{[\omega_{j,h}^n]_-^2\right\} \\
&\quad + \int_{\Omega^*} \epsilon_h^n |\nabla V_h^n|^2 + \int_\Omega \overline{\rho}_h^n |u_h^n|^2 + \tfrac{2\vartheta-1}{2} \sum_{k=1}^n \int_\Omega \left|\nabla\phi_h^k - \nabla\phi_h^{k-1}\right|^2 \\
&\quad + \sum_{k=1}^n \int_{\Omega^*} \epsilon_h^{k-1} \left|\nabla V_h^k - \nabla V_h^{k-1}\right|^2 + \tau \sum_{k=1}^n \int_\Omega \left|\nabla\mu_{\phi,h}^k\right|^2 + \alpha\tau \sum_{k=1}^n \int_{\partial\Omega} \mathcal{I}_h\left\{\left|\partial_\tau^- \phi_h^k\right|^2\right\} \\
&\quad + \tau \sum_{k=1}^n \int_\Omega 2\mathcal{I}_h\left\{\eta(\phi_h^k)\right\} \left|Du_h^k\right|^2 \\
&\quad + \tau \sum_{k=1}^n \sum_{j=1}^K \int_\Omega \left(\Xi_\nu[\omega_{j,h}^k]\nabla\left(\mu_{\omega_j,h}^k + z_j V_h^k\right)\right) \cdot \nabla\left(\mu_{\omega_j,h}^k + z_j V_h^k\right) \leq C\,, \qquad (3.16)
\end{aligned}$$

for $n \geq 1$, *where the abbreviation* $\mu_{\omega_i,h}^n := \mathcal{I}_h\left\{g_\nu'(\omega_{i,h}^n) + \beta_i(\phi_h^n)\right\}$ $(i = 1, ..., K)$ *for the discrete chemical potentials of the species was used.*

Proof We start by testing (2.12a) by $\mu_{\phi,h}^n$, (2.12b) by $\partial_\tau^- \phi_h^n$, (2.12c) by the sum of the chemical potential and the electrostatic potential $\mu_{\omega_i,h}^n + z_i V_h^n = \mathcal{I}_h\left\{g_\nu'(\omega_{i,h}^n) + \beta_i(\phi_h^n) + z_i V_h^n\right\}$, and (2.12e) by u_h^n. Adding the results and applying Young's inequality yields

$$\begin{aligned}
0 \geq\ & \tfrac{1}{2} \int_\Omega \partial_\tau^- |\nabla\phi_h^n|^2 + \int_\Omega \mathcal{I}_h\{\partial_\tau^- W(\phi_h^n)\} + \int_{\partial\Omega} \mathcal{I}_h\{\partial_\tau^- \gamma_{fs}(\phi_h^n)\} \\
&+ \sum_{i=1}^K \int_\Omega \mathcal{I}_h\{\partial_\tau^- g_\nu(\omega_{i,h}^n)\} + \sum_{i=1}^K \int_\Omega \mathcal{I}_h\left\{\partial_\tau^- \beta_i(\phi_h^n)\omega_{i,h}^{n-1}\right\} + \sum_{i=1}^K \int_\Omega \mathcal{I}_h\{\beta_i(\phi_h^n)\partial_\tau^- \omega_{i,h}^n\} \\
&+ \tfrac{1}{2} \int_{\Omega^*} \partial_\tau^- \epsilon_h^n |\nabla V_h^n|^2 + \tfrac{1}{2} \int_{\Omega^*} \epsilon_h^{n-1} \partial_\tau^- |\nabla V_h^n|^2 + \tfrac{1}{2} \int_\Omega \partial_\tau^- \left(\overline{\rho}_h^n |u_h^n|^2\right) \\
&+ \tfrac{2\vartheta-1}{2\tau} \int_\Omega \left|\nabla\phi_h^n - \nabla\phi_h^{n-1}\right|^2 + \tfrac{1}{2\tau} \int_{\Omega^*} \epsilon_h^{n-1} \left|\nabla V_h^n - \nabla V_h^{n-1}\right|^2 \\
&+ \int_\Omega \left|\nabla\mu_{\phi,h}^n\right|^2 + \alpha \int_{\partial\Omega} \mathcal{I}_h\left\{\left|\partial_\tau^- \phi_h^n\right|^2\right\} + \int_\Omega 2\mathcal{I}_h\left\{\eta(\phi_h^n)\right\} |Du_h^n|^2 \\
&+ \sum_{i=1}^K \int_\Omega \left(\Xi_\nu[\omega_{i,h}^n]\nabla(\mu_{\omega_i,h}^n + z_i V_h^n)\right) \cdot \nabla(\mu_{\omega_i,h}^n + z_i V_h^n) \\
&- \sum_{i=1}^K \int_\Omega \mathcal{I}_h\left\{R_{i,h}^n(\mu_{\omega_i,h}^n + z_i V_h^n)\right\} - \int_{\Omega^*} \partial_\tau^- \left(\epsilon_h^n \nabla V_h^n\right) \cdot \nabla \overline{V}_h^n \\
&+ \int_\Omega \mathcal{I}_h\left\{\sum_{i=1}^K z_i \partial_\tau^- \omega_{i,h}^n \overline{V}_h^n\right\}. \qquad (3.17)
\end{aligned}$$

The first three lines in (3.17) are the time difference quotient of the discrete energy. As the terms in lines four to six are nonnegative, we have to focus on the treatment of the last three terms. Recalling the definition of $R_{i,h}$ from (2.11), we obtain the identity

$$-\sum_{i=1}^{K} R_{i,h}^n(\mu_{\omega_i,h}^n + z_i V_h^n) = \left[\exp\left(\sum_{\zeta_j<0} |\zeta_j|\,(\mu_{\omega_j,h}^n + z_j V_h^n)\right) - \exp\left(\sum_{\zeta_j\geq 0} \zeta_j(\mu_{\omega_j,h}^n + z_j V_h^n)\right)\right] \times \left(\sum_{\zeta_i<0} |\zeta_i|\left(\mu_{\omega_i,h}^n + z_i V_h^n\right) - \sum_{\zeta_i\geq 0} \zeta_i(\mu_{\omega_i,h}^n + z_i V_h^n)\right) \tag{3.18}$$

on every vertex of the underlying triangulation. Since exp is a monotone increasing function, (3.18) provides $-\sum_{i=1}^K \int_\Omega \mathcal{I}_h\left\{R_{i,h}^n(\mu_{\omega_i,h}^n + z_i V_h^n)\right\} \geq 0$. Therefore, we infer from (3.17) after a discrete integration with respect to time

$$\begin{aligned}
&\tfrac{1}{2}\int_\Omega \left|\nabla\phi_h^n\right|^2 + \int_\Omega \mathcal{I}_h\{W(\phi_h^n)\} + \int_{\partial\Omega} \mathcal{I}_h\{\gamma_{fs}(\phi_h^n)\} + \sum_{i=1}^K \int_\Omega \mathcal{I}_h\{g_\nu(\omega_{i,h}^n)\} \\
&\quad + \sum_{i=1}^K \int_\Omega \mathcal{I}_h\{\beta_i(\phi_h^n)\omega_{i,h}^n\} + \tfrac{1}{2}\int_{\Omega^*} \epsilon_h^n \left|\nabla V_h^n\right|^2 + \tfrac{1}{2}\int_\Omega \overline{\rho}_h^n \left|u_h^n\right|^2 \\
&\quad + \tfrac{2\vartheta-1}{2}\sum_{k=1}^n \int_\Omega \left|\nabla\phi_h^k - \nabla\phi_h^{k-1}\right|^2 + \tfrac{1}{2}\sum_{k=1}^n \int_{\Omega^*} \epsilon_h^{k-1}\left|\nabla V_h^k - \nabla V_h^{k-1}\right|^2 \\
&\quad + \tau\sum_{k=1}^n \int_\Omega \left|\nabla\mu_{\phi,h}^k\right|^2 + \alpha\tau\sum_{k=1}^n \int_{\partial\Omega} \mathcal{I}_h\left\{\left|\partial_\tau^- \phi_h^k\right|^2\right\} + \tau\sum_{k=1}^n \int_\Omega 2\mathcal{I}_h\left\{\eta(\phi_h^k)\right\}\left|Du_h^k\right|^2 \\
&\quad + \tau\sum_{k=1}^n \sum_{i=1}^K \int_\Omega \left(\Xi_\nu[\omega_{i,h}^k]\nabla(\mu_{\omega_i,h}^k + z_i V_h^k)\right)\cdot\nabla(\mu_{\omega_i,h}^k + z_i V_h^k) \\
&\quad \leq C(\phi_h^0, (\omega_h^0)^K, u_h^0) \\
&\quad + \tau\sum_{k=1}^n \int_{\Omega^*} \partial_\tau^-\left(\epsilon_h^k \nabla V_h^k\right)\cdot\nabla\overline{V}_h^k - \tau\sum_{k=1}^n \int_\Omega \mathcal{I}_h\left\{\sum_{i=1}^K z_i \partial_\tau^- \omega_{i,h}^k \overline{V}_h^k\right\}
\end{aligned} \tag{3.19}$$

As $\omega_{i,h}$ may become negative, we have to absorb $\int_\Omega \mathcal{I}_h\left\{\beta_i(\phi_h^n)\omega_{i,h}^n\right\}$ in $\int_\Omega \mathcal{I}_h\left\{g_\nu(\omega_{i,h}^n)\right\}$. For this reason, we consider a dual basis to the nodes $\{x_j\}_{j=1,\ldots,\dim U_h}$ which is denoted by $\{\chi_{h,j}\}_{j=1,\ldots,\dim U_h}$. Furthermore, we define positive weights $\lambda_j := \int_\Omega \chi_{h,j}$ for all $j \in \{1, \ldots, \dim U_h\}$. We compute

$$\begin{aligned}
\tfrac{1}{2}\int_\Omega \mathcal{I}_h\{g_\nu(\omega_{i,h}^n)\} &= \tfrac{1}{2}\sum_{j=1}^{\dim U_h} \lambda_j g_\nu(\omega_{i,h}^n(P_j)) = \tfrac{1}{2}\sum_{j\,:\,\omega_{i,h}^n(P_j)\geq 0} \lambda_j g_\nu(\omega_{i,h}^n(P_j)) \\
&\quad + \tfrac{1}{2}\sum_{j\,:\,\omega_{i,h}^n(P_j)<0} \lambda_j g_\nu(\omega_{i,h}^n(P_j)) \geq -C + \frac{1}{4\nu}\int_\Omega \mathcal{I}_h\left\{[\omega_{i,h}^n]_-^2\right\},
\end{aligned} \tag{3.20}$$

due to (2.4a). Applying Young's inequality finally shows that

$$\tfrac{1}{2}\int_\Omega \mathcal{I}_h\{g_\nu(\omega_{i,h}^n)\} + \int_\Omega \mathcal{I}_h\{\beta_i(\phi_h^n)\omega_{i,h}^n\} + C \geq \left(\tfrac{1}{4\nu} - \delta\right)\int_\Omega \mathcal{I}_h\left\{[\omega_{i,h}^n]_-^2\right\} \tag{3.21}$$

holds true for $i = 1, ..., K$ with some C and with $0 < \delta \ll 1$ independent of the discrete solutions. Therefore, the left-hand side of (3.16) is bounded from above by

$$C + C\left(\tau \sum_{k=1}^{n} \int_{\Omega^*} \partial_\tau^- \left(\epsilon_h^k \nabla V_h^k\right) \cdot \nabla \overline{V}_h^k - \tau \sum_{k=1}^{n} \int_{\Omega} \mathcal{I}_h \left\{ \sum_{i=1}^{K} z_i \partial_\tau^- \omega_{i,h}^k \overline{V}_h^k \right\}\right). \quad (3.22)$$

Although the last two terms look similar to (2.12d), they do not vanish in general, as $\overline{V}_h^k \neq 0$ on Γ_D. Applying the cutoff function Π_{c_Γ} defined in (3.5), we introduce the function $\overline{\mathcal{V}}_h^k := \Pi_{c_\Gamma}(\overline{V}_h^k)$. As $\overline{\mathcal{V}}_h^k = 0$ on Γ_D and $\overline{\mathcal{V}}_h^k = \overline{V}_h^k$ on Ω, we may use (2.12d) to rewrite (3.22) as

$$C + C\tau \sum_{k=1}^{n} \int_{\Omega^*} \partial_\tau^- \left(\epsilon_h^k \nabla V_h^k\right) \cdot \nabla \left(\overline{V}_h^k - \overline{\mathcal{V}}_h^k\right). \quad (3.23)$$

Applying a discrete partial integration with respect to time and Young's inequality, we compute

$$\begin{aligned}
& C\tau \sum_{k=1}^{n} \int_{\Omega^*} \partial_\tau^- \left(\epsilon_h^k \nabla V_h^k\right) \cdot \nabla \left(\overline{V}_h^k - \overline{\mathcal{V}}_h^k\right) \\
\leq\ & C\tau \int_{\Omega^*} \epsilon_h^n \nabla V_h^n \cdot \nabla \left(\overline{V}_h^n - \overline{\mathcal{V}}_h^n\right) - C\tau \sum_{k=1}^{n} \int_{\Omega^*} \left(\epsilon_h^{k-1} \nabla V_h^{k-1}\right) \cdot \nabla \partial_\tau^- \left(\overline{V}_h^k - \overline{\mathcal{V}}_h^k\right) \\
& - C\tau \int_{\Omega^*} \epsilon_h^0 \nabla V_h^0 \cdot \nabla \left(\overline{V}_h^0 - \overline{\mathcal{V}}_h^0\right) \\
\leq\ & \tfrac{1}{4} \int_{\Omega^*} \epsilon_h^n \left|\nabla V_h^n\right|^2 + C\tau \int_{\Omega^*} \left|\nabla \overline{V}_h^n\right|^2 + C\tau \int_{\Omega^*} \left|\nabla \overline{\mathcal{V}}_h^n\right|^2 + C\tau \sum_{k=1}^{n} \int_{\Omega^*} \epsilon_h^{k-1} \left|\nabla V_h^{k-1}\right|^2 \\
& + C\tau \sum_{k=1}^{n} \int_{\Omega^*} \left|\nabla \partial_\tau^- \overline{V}_h^k\right|^2 + C\tau \sum_{k=1}^{n} \int_{\Omega^*} \left|\nabla \partial_\tau^- \overline{\mathcal{V}}_h^k\right|^2 + C\tau \int_{\Omega^*} \epsilon_h^0 \left|\nabla V_h^0\right|^2 \\
& + C\tau \int_{\Omega^*} \left|\nabla \overline{V}_h^0\right|^2 + C\tau \int_{\Omega^*} \left|\nabla \overline{\mathcal{V}}_h^0\right|^2, \quad (3.24)
\end{aligned}$$

as ϵ is bounded. Recalling the estimates on Π_{c_Γ} (see Lemma 3.1) and the regularity assumptions on $\overline{V}_h$ (see (E6)), we complete the proof by absorbing the first term on the right-hand side and by applying a discrete version of Gronwall's lemma (cf., e.g. [23]). □

Using the a priori estimate stated in the lemma above, we will now establish the existence of discrete solutions. For this purpose, we need an auxiliary result which was proven in Lemma 2.11 in [17].

Lemma 3.3 *Let ϵ satisfy (E5). Then*

$$\epsilon[a](x) + \epsilon[b](x) - \epsilon'_{DQ}(a, b)b \geq 0 \quad (3.25)$$

holds true for every $a, b \in \mathbb{R}$ and $x \in \Omega$.

Lemma 3.4 *Let the Assumptions (E1)–(E7) hold true. Then, for given*

$$(\phi_h^{n-1}, (\omega_h^{n-1})^K, V_h^{n-1} - \overline{V}_h^{n-1}, u_h^{n-1}) \in U_h \times (U_h)^K \times U_{h,0}^* \times \boldsymbol{W}_{h,\mathrm{div}}\,,$$

there exists at least one tuple $(\phi_h^n, \mu_{\phi,h}^n, (\omega_h^n)^K, V_h^n - \overline{V}_h^n, u_h^n) \in U_h \times U_h \times (U_h)^K \times U_{h,0}^* \times \boldsymbol{W}_{h,\mathrm{div}}$ *solving* (2.12).

Proof The structure of the (2.12d) and (2.12b) provides the existence of unique V_h^n and $\mu_{\phi,h}^n$ for any given ϕ_h^n and $(\omega_h^n)^K$. Consequently, we may treat V_h^n and $\mu_{\phi,h}^n$ as functions depending on the quantities ϕ_h^n and $(\omega_h^n)^K$. In general, we will write $V_h(\phi_h, (\omega_h)^K) \in U_h^*$ and $\mu_{\phi,h}(\phi_h, (\omega_h)^K) \in U_h$ for the solutions of

$$\int_{\Omega^*} \mathcal{I}_h\{\epsilon[\phi_h](\mathbf{x})\}\nabla V_h(\phi_h, (\omega_h)^K) \cdot \nabla\theta_h = \int_\Omega \mathcal{I}_h\left\{\sum_{j=1}^K z_j\omega_{j,h}\theta_h\right\} \tag{3.26}$$

for all $\theta_h \in U_{h,0}^*$, subjected to the constraint $V_h(\phi_h, (\omega_h)^K) = \overline{V}_h^n$ on Γ_D and

$$\begin{aligned}\int_\Omega \mathcal{I}_h\left\{\mu_{\phi,h}(\phi_h, (\omega_h)^K)\theta_h\right\} = &\int_\Omega (\vartheta\nabla\phi_h + (1-\vartheta)\nabla\phi_h^{n-1}) \cdot \nabla\theta_h + \int_\Omega \mathcal{I}_h\left\{W_h'(\phi_h, \phi_h^{n-1})\theta_h\right\}\\ &+ \int_{\partial\Omega} \mathcal{I}_h\left\{\gamma_{fs,DQ}'(\phi_h, \phi_h^{n-1})\theta_h\right\} + \alpha\tau^{-1}\int_{\partial\Omega} \mathcal{I}_h\left\{(\phi_h - \phi_h^{n-1})\theta_h\right\}\\ &+ \int_\Omega \mathcal{I}_h\left\{\sum_{j=1}^K \beta_{j,DQ}'(\phi_h, \phi_h^{n-1})\omega_{j,h}^{n-1}\theta_h\right\}\\ &- \tfrac{1}{2}\int_\Omega \mathcal{I}_h\left\{\epsilon_{DQ}'(\phi_h, \phi_h^{n-1})\theta_h\right\}\left|\nabla V_h(\phi_h, (\omega_h)^K)\right|^2 \forall\theta_h \in U_h\,. \end{aligned} \tag{3.27}$$

To prove the existence of the remaining quantities, we proceed as follows. We assume the nonexistence of solutions and use Brouwer's fixed point theorem to construct a contradiction. To omit clumsy notation, we assume w.l.o.g. $\int_\Omega \phi_h^n = \int_\Omega \phi_h^{n-1} = 0$, i.e., we look for solutions Φ_h^n in the space $S_h \subset U_h$. We define an inner product $((.,.))$ on $S_h \times (U_h)^K \times \boldsymbol{W}_{h,\mathrm{div}}$ via

$$(((\phi_h, (\omega_h)^K, u_h), (\psi_h, (\theta_h)^K, w_h))) := \int_\Omega \mathcal{I}_h\{\phi_h\psi_h\} + \sum_{j=1}^K \int_\Omega \mathcal{I}_h\{\omega_{j,h}\theta_{j,h}\} + \int_\Omega u_h \cdot w_h \tag{3.28}$$

for all $(\phi_h, (\omega_h)^K, u_h), (\psi_h, (\theta_h)^K, w_h) \in S_h \times (U_h)^K \times \boldsymbol{W}_{h,\mathrm{div}}$. Given $(\phi_h^{n-1}, (\omega_h^{n-1})^K, u_h^{n-1}) \in S_h \times (U_h)^K \times \boldsymbol{W}_{h,\mathrm{div}}$, we define a mapping $\mathcal{H} := \left(\mathcal{F}_\phi, \{\mathcal{F}_{\omega_i}\}_{i=1,\dots,K}, \boldsymbol{\mathcal{F}}_u\right)$ mapping $S_h \times (U_h)^K \times \boldsymbol{W}_{h,\mathrm{div}}$ onto itself. These functions are the residual of (2.12) and defined via

$$\begin{aligned}\int_\Omega \mathcal{I}_h\left\{\mathcal{F}_\phi(\phi_h, (\omega_h)^K, u_h)\psi_h\right\} = &\int_\Omega \mathcal{I}_h\left\{(\phi_h - \phi_h^{n-1})\psi_h\right\} - \tau\int_\Omega \phi_h^{n-1}u_h^{n-1} \cdot \nabla\psi_h\\ + \tau\int_\Omega &\left(\tau(\min\overline{\rho}_h^{n-1})^{-1}|\phi_h^{n-1}|^2 + 1\right)\nabla\mu_{\phi,h}(\phi_h, (\omega_h)^K) \cdot \nabla\psi_h\,, \end{aligned} \tag{3.29a}$$

$$\int_\Omega \mathcal{I}_h\Big\{\mathcal{F}_{\omega_i}(\phi_h,(\omega_h)^K,u_h)\theta_h\Big\} = \int_\Omega \mathcal{I}_h\Big\{(\omega_{i,h}-\omega_{i,h}^{n-1})\theta_h\Big\} - \tau\int_\Omega \omega_{i,h}^{n-1}u_h^{n-1}\cdot\nabla\theta_h$$
$$+\ \tau^2 K\int_\Omega (\min\overline{\rho}_h^{n-1})^{-1}|\omega_{i,h}|^2\nabla\mathcal{I}_h\Big\{g_\nu'(\omega_{i,h})+\beta_i(\phi_h)+z_iV_h(\phi_h,(\omega_h)^K)\Big\}\cdot\nabla\theta_h$$
$$+\ \tau\int_\Omega\Big(\Xi_\nu[\omega_{i,h}]\nabla\mathcal{I}_h\Big\{g_\nu'(\omega_{i,h})+\beta_i(\phi_h)+z_iV_h(\phi_h,(\omega_h)^K)\Big\}\Big)\cdot\nabla\theta_h$$
$$-\tau\int_\Omega \mathcal{I}_h\Big\{R_{i,h}(\phi_h,(\omega_h)^K,V_h(\phi_h,(\omega_h)^K))\theta_h\Big\}, \tag{3.29b}$$

$$\int_\Omega \boldsymbol{\mathcal{F}}_u(\phi_h,(\omega_h)^K,u_h)\cdot w_h = \int_\Omega \tfrac{1}{2}(\overline{\rho}_h+\overline{\rho}_h^{n-1})(u_h-u_h^{n-1})\cdot w_h + \tfrac{1}{2}\int_\Omega(\overline{\rho}_h-\overline{\rho}_h^{n-1})u_h^{n-1}\cdot w_h$$
$$+\ \tfrac{1}{2}\tau\int_\Omega\overline{\rho}_h\Big((\nabla u_h)^T\cdot w_h\Big)\cdot u_h^{n-1} - \tfrac{1}{2}\tau\int_\Omega\overline{\rho}_h\Big((\nabla w_h)^T\cdot u_h\Big)\cdot u_h^{n-1}$$
$$+\ \tfrac{1}{2}\tau\int_\Omega\tfrac{\delta\overline{\rho}}{\delta\phi}\Big((\nabla u_h)^T\cdot w_h\Big)\cdot\nabla\mu_{\phi,h}(\phi_h,(\omega_h)^K) - \tfrac{1}{2}\tau\int_\Omega\tfrac{\delta\overline{\rho}}{\delta\phi}\Big((\nabla w_h)^T\cdot u_h\Big)\cdot\nabla\mu_{\phi,h}(\phi_h,(\omega_h)^K)$$
$$+\ \tau\int_\Omega 2\mathcal{I}_h\{\eta(\phi_h)\}Du_h : Dw_h + \tau\int_\Omega\phi_h^{n-1}\nabla\mu_{\phi,h}(\phi_h,(\omega_h)^K)\cdot w_h$$
$$+\ \tau\sum_{j=1}^K\int_\Omega\omega_{j,h}^{n-1}\nabla\mathcal{I}_h\Big\{g_\nu'(\omega_{j,h})+\beta_j(\phi_h)+z_jV_h(\phi_h,(\omega_h)^K)\Big\}\cdot w_h\,, \tag{3.29c}$$

for all $\psi_h\in S_h$, $\theta_h\in U_h$, $w_h\in\boldsymbol{W}_{h,\mathrm{div}}$, and $i\in\{1,\ldots,K\}$ with $\overline{\rho}_h := \mathcal{I}_h\{\overline{\rho}(\phi_h)\}$. Therefore, the existence of a root to $\mathcal{H}$ is equivalent to the existence of solutions to (2.12). Assuming $\mathcal{H}\neq 0$ on

$$B_R := \Big\{(\psi_h,(\theta_h)^K,w_h)\in S_h\times(U_h)^K\times\boldsymbol{W}_{h,\mathrm{div}} : \Big|\!\Big|\!\Big|(\psi_h,(\theta_h)^K,w_h)\Big|\!\Big|\!\Big|\le R\Big\} \tag{3.30}$$

with $|\!|\!|.|\!|\!| = \sqrt{((.,.))}$, the continuous mapping $\mathcal{G} : B_R\to B_R$ defined by

$$\mathcal{G}\Big(\psi_h,(\theta_h)^K,w_h\Big) := -R\frac{\mathcal{H}(\psi_h,(\theta_h)^K,w_h)}{\Big|\!\Big|\!\Big|\mathcal{H}(\psi_h,(\theta_h)^K,w_h)\Big|\!\Big|\!\Big|} \tag{3.31}$$

has—due to Brouwer's fixed point theorem—at least one fixed point, which we denote by $(\hat{\phi}_h,(\hat{\omega}_h)^K,\hat{u}_h)$. We will now show that for a suitable choice of $\hat{\psi}_h$, $(\hat{\theta}_h)^K$, and $\hat{\mathbf{w}}_h$

$$0 < (((\hat{\phi}_h,(\hat{\omega}_h)^K,\hat{u}_h),(\hat{\psi}_h,(\hat{\theta}_h)^K,\hat{w}_h))) < 0 \tag{3.32}$$

holds true for R large enough. This contradiction then provides the desired result. We choose $\hat{\psi}_h$, $(\hat{\theta}_h)^K$, and $\hat{w}_h$ as follows. Abbreviating $V_h(\hat{\phi}_h,(\hat{\omega}_h)^K)$ by $\hat{V}_h$ and the chemical potential $\mu_{\phi,h}(\hat{\phi}_h,(\hat{\omega}_h)^K)$ by $\hat{\mu}_{\phi,h}$, we define

$$\hat{\psi}_h := \hat{\mu}_{\phi,h} - \tfrac{1}{|\Omega|}\int_\Omega\hat{\mu}_{\phi,h}\in S_h\,, \tag{3.33a}$$
$$\hat{\theta}_{i,h} := \mathcal{I}_h\Big\{g_\nu'(\hat{\omega}_{i,h})+\beta_i(\hat{\phi}_h)+z_i\hat{V}_h\Big\}\in U_h\,, \tag{3.33b}$$
$$\hat{w}_h := \hat{u}_h\in\boldsymbol{W}_{h,\mathrm{div}}\,. \tag{3.33c}$$

We start by proving the first inequality in (3.32). As $\hat{\phi}_h$ has zero mean, we apply Young's inequality with $0 < \delta \ll 1$ and compute

$$\begin{aligned}
&\int_\Omega \mathcal{I}_h\Big\{\hat{\phi}_h\hat{\psi}_h\Big\} = \int_\Omega \mathcal{I}_h\Big\{\hat{\phi}_h\hat{\mu}_{\phi,h}\Big\}\\
\geq\ & \vartheta\int_\Omega |\nabla\hat{\phi}_h|^2 - \delta\int_\Omega |\nabla\hat{\phi}_h|^2 - C_\delta\int_\Omega \left|\nabla\phi_h^{n-1}\right|^2 + \int_\Omega \mathcal{I}_h\Big\{W_h'(\hat{\phi}_h,\phi_h^{n-1})\hat{\phi}_h\Big\}\\
&+\int_{\partial\Omega}\mathcal{I}_h\Big\{\gamma_{fs,DQ}'(\hat{\phi}_h,\phi_h^{n-1})\hat{\phi}_h\Big\} + \tfrac{\alpha}{2\tau}\int_{\partial\Omega}\mathcal{I}_h\Big\{|\hat{\phi}_h|^2+|\hat{\phi}_h-\phi_h^{n-1}|^2-\left|\phi_h^{n-1}\right|^2\Big\}\\
&+\int_\Omega \mathcal{I}_h\left\{\sum_{j=1}^K \beta_{j,DQ}'(\hat{\phi}_h,\phi_h^{n-1})\omega_{j,h}^{n-1}\hat{\phi}_h\right\} - \tfrac{1}{2}\int_\Omega \mathcal{I}_h\Big\{\epsilon_{DQ}'(\hat{\phi}_h,\phi_h^{n-1})\hat{\phi}_h\Big\}\left|\nabla\hat{V}_h\right|^2\\
=:\ & I_\phi + II_\phi + III_\phi + IV_\phi + V_\phi + VI_\phi + VII_\phi + VIII_\phi\,. \qquad (3.34)
\end{aligned}$$

Obviously, we have $III_\phi \geq -C$, $VI_\phi \geq -C$, and $IV_\phi \geq -C$ due to (W1). From (E3) and (E4), we obtain also $V_\phi \geq -C$ and $VII_\phi \geq -C$.
As g_ν is a convex function, we obtain for $i = 1, ..., K$

$$\begin{aligned}
\int_\Omega \mathcal{I}_h\Big\{\hat{\omega}_{i,h}\hat{\theta}_{i,h}\Big\} &= \int_\Omega \mathcal{I}_h\Big\{\hat{\omega}_{i,h}(g_\nu'(\hat{\omega}_{i,h}) + \beta_i(\hat{\phi}_h) + z_i\hat{V}_h)\Big\}\\
&\geq \int_\Omega \mathcal{I}_h\big\{g_\nu(\hat{\omega}_{i,h}) - g_\nu(0)\big\} + \int_\Omega \mathcal{I}_h\Big\{\beta_i(\hat{\phi})\hat{\omega}_{i,h}\Big\}\\
&\quad + \int_\Omega \mathcal{I}_h\Big\{\hat{\omega}_{i,h}z_i\hat{V}_h\Big\} := I_{\omega_i} + II_{\omega_i} + III_{\omega_i}. \qquad (3.35)
\end{aligned}$$

Recalling the arguments used in the proof of Lemma 3.2 to deduce (3.21) yields $\frac{1}{2}I_{\omega_i} + II_{\omega_i} \geq -C$.
Using $\overline{V}_h^n - \Pi_{c_\Gamma}(\overline{V}_h^n) \equiv 0$ on Ω, $\hat{V}_h - \overline{V}_h^n + \Pi_{c_\Gamma}(\overline{V}_h^n) \equiv 0$ on Γ_D and (3.26), we compute

$$\begin{aligned}
&\sum_{i=1}^K III_{\omega_i} = \sum_{i=1}^K\int_\Omega \mathcal{I}_h\Big\{\hat{\omega}_{i,h}z_i\Big(\hat{V}_h - \overline{V}_h^n + \Pi_{c_\Gamma}(\overline{V}_h^n)\Big)\Big\}\\
&= \int_{\Omega^*}\mathcal{I}_h\Big\{\epsilon[\hat{\phi}_h](x)\Big\}\nabla\hat{V}_h\cdot\nabla\hat{V}_h - \int_{\Omega^*\setminus\Omega}\mathcal{I}_h\Big\{\epsilon[\hat{\phi}_h](x)\Big\}\nabla\hat{V}_h\cdot\nabla\Big(\overline{V}_h^n - \Pi_{c_\Gamma}(\overline{V}_h^n)\Big)\,. \qquad (3.36)
\end{aligned}$$

Combining (3.36) and $VIII_\phi$ shows

$$\begin{aligned}
&\sum_{i=1}^K III_{\omega_i} + VIII_\phi = \tfrac{1}{2}\int_\Omega \mathcal{I}_h\Big\{\epsilon[\hat{\phi}_h](x) + \epsilon[\phi_h^{n-1}](x) - \epsilon_{DQ}'(\hat{\phi}_h,\phi_h^{n-1})\phi_h^{n-1}\Big\}\left|\nabla\hat{V}_h\right|^2\\
&+\int_{\Omega^*\setminus\Omega}\mathcal{I}_h\Big\{\epsilon[\hat{\phi}_h](x)\Big\}\nabla\hat{V}_h\cdot\nabla\hat{V}_h - \int_{\Omega^*\setminus\Omega}\mathcal{I}_h\Big\{\epsilon[\hat{\phi}_h](x)\Big\}\nabla\hat{V}_h\cdot\nabla\Big(\overline{V}_h^n - \Pi_{c_\Gamma}(\overline{V}_h^n)\Big). \qquad (3.37)
\end{aligned}$$

According to Lemma 3.3, the first term is nonnegative. Due to Young's inequality and Lemma 3.1, the first two terms are bounded from below by $-C$ depending on $\overline{V}_h^n$ but not on the fixed point.

Noting $\int_\Omega |\hat{u}_h|^2 \cdot \hat{w}_h = \int_\Omega |\hat{u}_h|^2$, we deduce

$$(((\hat{\phi}_h, (\hat{\omega}_h)^K, \hat{u}_h), (\hat{\psi}_h, (\hat{\theta}_h)^K, \hat{w}_h))) \geq (\vartheta - \delta) \int_\Omega \left|\nabla \hat{\phi}_h\right|^2 + \tfrac{1}{2} \sum_{j=1}^K \int_\Omega \mathcal{I}_h\{g_\nu(\hat{\omega}_{j,h})\} + \int_\Omega |\hat{u}_h|^2 - C\,. \tag{3.38}$$

As $g_\nu(s) \geq |s| - C$ for $s \in \mathbb{R}$ and $\hat{\phi}_h \in S_h$, we may use the equivalence of norms on finite dimensional spaces to deduce the first inequality in (3.32) for R large enough. To prove the second inequality in (3.32), we follow the lines of the proof of Lemma 3.2 to deduce

$$\begin{aligned}
&(((\mathcal{H}(\hat{\phi}_h, (\hat{\omega}_h)^K, \hat{u}_h), (\hat{\psi}_h, (\hat{\theta}_h)^K, \hat{\mathbf{w}}_h))) \\
&\geq -C + \tfrac{1}{2} \int_\Omega \left|\nabla \hat{\phi}_h\right|^2 + \tfrac{1}{2} \sum_{j=1}^K \int_\Omega \mathcal{I}_h\{g_\nu(\hat{\omega}_{j,h})\} + \tfrac{1}{2} \int_{\Omega^*} \mathcal{I}_h\left\{\epsilon[\hat{\phi}_h](x)\right\} \left|\nabla \hat{V}_h\right|^2 \\
&\quad + \tfrac{1}{2} \min_{s\in\mathbb{R}} \overline{\rho}(s) \int_\Omega |\hat{u}_h|^2 - \int_{\Omega^*} \left(\mathcal{I}_h\left\{\epsilon[\hat{\phi}_h](x)\right\} \nabla \hat{V}_h - \mathcal{I}_h\left\{\epsilon[\phi_h^{n-1}](\mathbf{x})\right\} \nabla V_h^{n-1}\right) \cdot \nabla \overline{V}_h^n \\
&\quad + \sum_{j=1}^K \int_\Omega \mathcal{I}_h\left\{z_j(\hat{\omega}_{j,h} - \omega_{j,h}^{n-1}) \overline{V}_h^n\right\} \\
&\geq -C + \tfrac{1}{2} \int_\Omega \left|\nabla \hat{\phi}_h\right|^2 + \tfrac{1}{2} \sum_{j=1}^K \int_\Omega \mathcal{I}_h\{g_\nu(\hat{\omega}_{j,h})\} \\
&\quad + \tfrac{1}{2} \min_{s\in\mathbb{R}} \overline{\rho}(s) \int_\Omega |\hat{u}_h|^2 - C \sum_{j=1}^K \int_\Omega \mathcal{I}_h\{|\hat{\omega}_{j,h}|\}\,,
\end{aligned} \tag{3.39}$$

as $\overline{V}_h^n$ is sufficiently regular (cf. (E6)). As g_ν has superlinear growth, $\frac{1}{4} g_\nu(s) \geq C|s|$ holds true for s larger than some critical value $\tilde{\omega}$ which is independent of R. Hence,

$$\begin{aligned}
\tfrac{1}{4} \int_\Omega \mathcal{I}_h\{g_\nu(\hat{\omega}_{j,h})\} - C \int_\Omega \mathcal{I}_h\{|\hat{\omega}_{j,h}|\} &\geq -C \int_\Omega \mathcal{I}_h\{\min\{\tilde{\omega}, |\hat{\omega}_{j,h}|\}\} - C \\
&\geq -C|\Omega|\tilde{\omega} - C
\end{aligned} \tag{3.40}$$

holds true for $j = 1, ..., K$. Therefore, similar arguments as in the last step imply the positivity of the right-hand side for R large enough. Recalling that $(\hat{\phi}_h, (\hat{\omega}_h)^K, \hat{u}_h)$ is a fixed point of $\mathcal{G}$, (3.31) completes the proof. □

4 Numerical experiments

For practical computations, the finite element scheme (2.12) is implemented in the framework of the inhouse code `EconDrop` which is written in `C++` (cf. [2, 5, 13]). In this section, we present and discuss simulations based on the presented scheme. In Section 4.1, we use the simulation of a falling droplet as an example to illustrate the effect of the different discretization techniques introduced in Section 2 to reduce the numerical dissipation. In Sections 4.2 and 4.3, we present simulations of ion induced droplet deformations to validate the basic functionality of the model and the discrete scheme.

4.1 Numerical dissipation

Simulations published in [12] already indicated that numerical dissipation may affect the falling velocity of droplets. Generally, one may derive an energy inequality of the form

$$\text{energy}(t^n) \;+\; \text{dissipation} \;\leq\; \text{energy}(t^{n-1}) \;+\; \text{external forces}\,, \tag{4.1}$$

i.e., external forces may increase the energy of the system, while dissipation withdraws energy from the system. As the energy of pure two-phase flows (in absence of dissolved species) consists of a kinetic term $\frac{1}{2}\int_\Omega \rho\,|u|^2$ and terms describing the fluid-fluid and fluid-wall contact energies (cf. (1.3)), an energy reduction may be obtained either by optimizing the shape of the droplet or by reducing the velocity.
The scheme presented in Section 2 includes several mechanisms to reduce the numerical dissipation and therefore the artificial loss of energy: First, the parameter ϑ allows to interpolate between time discretizations of the discrete Laplacian introducing a different amount of numerical dissipation. In particular, we combine the following identities.

$$\nabla\phi_h^n \cdot \nabla\partial_\tau^-\phi_h^n \;=\; \tfrac{1}{2\tau}\left|\nabla\phi_h^n\right|^2 + \tfrac{1}{2\tau}\left|\nabla\phi_h^n - \nabla\phi_h^{n-1}\right|^2 - \tfrac{1}{2\tau}\left|\nabla\phi_h^{n-1}\right|^2 \tag{4.2a}$$

$$\tfrac{1}{2}\left(\nabla\phi_h^n + \nabla\phi_h^{n-1}\right) \cdot \nabla\partial_\tau^-\phi_h^n \;=\; \tfrac{1}{2\tau}\left|\nabla\phi_h^n\right|^2 - \tfrac{1}{2\tau}\left|\nabla\phi_h^{n-1}\right|^2 . \tag{4.2b}$$

Secondly, the assumptions (W1)–(W5) allow for different approximations of W'. In particular, we will use a polynomial double-well potential with penalty term (cf. [12])

$$W(\phi) := \tfrac{1}{4}(1-\phi^2)^2 + \tfrac{1}{\delta'}\max\{|\phi|-1,\,0\}^2 \tag{4.3}$$

with $\delta' = 4\cdot 10^{-3}$ and compare the following approaches.

(CC) Given a convex-concave decomposition $W = W_{\text{conv}} + W_{\text{conc}}$, we set

$$W_h'(a,b) := W_{\text{conv}}'(a) + W_{\text{conc}}'(b)\,.$$

(DQ) We compute the difference quotient of the polynomial part and set

$$W_h'(a,b) := \tfrac{1}{4}\left(a^3+a^2b+ab^2+b^3\right) - \tfrac{1}{2}(a+b) + \tfrac{1}{\delta'}\,\tfrac{\mathrm{d}}{\mathrm{d}s}\Big|_{s=a}\max\{|s|-1,0\}^2\,.$$

(IM) Combining the ideas of (CC) and (DQ), we set

$$W_h'(a,b) := W'(a) + \tfrac{a-b}{2}\,.$$

While (DQ) is expected to be the least dissipative approximation, (IM) is constructed as an intermediate between (CC) and (DQ), i.e., starting from a suitable convex-concave decomposition of W, the derivative of the concave part is approximated using a difference quotient.
To investigate the influence of the numerical dissipation, we decide on a simple experiment. A comparison of (IM) and (DQ) in a more sophisticated setting can be found in [12]. Given the rectangular domain $(-1,1)\times(-1,5)$ filled with a fluid of mass density 1, we position a circular droplet with radius 0.3, barycenter at

$(0, 4)$ and mass density 3 (cf. Figure 2 and Table 1). We include gravity by adding $-\int_\Omega \overline{\rho}_h^n g e_{x_2} \cdot w$ with the gravitational acceleration $g = 10$ on the right-hand side of (2.12e), which results in the droplet falling downwards. By choosing a relatively high surface energy density $\sigma = 10$, we prevent the droplet from deforming. Therefore, tracking the position of its barycenter provides a good indication for the droplet's position.
The mesh is adaptive, i.e., it is relatively coarse in the pure fluids while providing a fine resolution in the interfacial area. It consists of simplices with diameter between approximately 0.067 and 0.008. Concerning the boundary conditions, $u = 0$ and $\nabla\phi \cdot n$ are imposed on $\partial\Omega \times \mathbb{R}^+$. For the remaining parameters, we refer to Table 1.

We start by investigating the influence of the time increment on the results computed using (DQ) and $\vartheta = 0.5$ which corresponds to the least dissipative scheme. For this reason, we track the droplet's barycenter and compute the kinetic energy $\mathcal{E}_{\text{kin}}(\phi_h^n, u_h^n) := \int_\Omega \mathcal{I}_h\{\rho(\phi_h^n)\}|u_h^n|^2$ of the system. As it turns out, the computed positions of the droplet vary only little when decreasing the time increment. The variations in the kinetic energy are slightly larger. However, Fig. 3 suggests that a further reduction of the time increment will not improve the results significantly. Therefore, the results based on (DQ) and $\vartheta = 0.5$ may serve as reference solutions in the comparison with the other approaches.
In the next step, we compare the results of different schemes for time increments $\tau = 1.0 \cdot 10^{-4}$ and $\tau = 2.5 \cdot 10^{-5}$. The results are depicted in Figs. 4 and 5. The differences between the results obtained with the most dissipative scheme ((CC), $\vartheta = 1.0$) and the least dissipative scheme are evident. As predicted by (4.1), larger numerical dissipation reduces the kinetic energy significantly and thereby inhibits large velocities. Consequently, different schemes compute different droplet positions. While the first, most dissipative scheme suggest a final droplet position at height 3 ($\tau = 1.0 \cdot 10^{-4}$) or height 2 ($\tau = 2.5 \cdot 10^{-4}$), respectively, the reference solutions yield approx. 0.6 as the height of the barycenter at time 2.
Concerning the impact of the aforementioned mechanisms, Figs. 4 and 5 indicate that using a discretization of W' which induces only little numerical dissipation is inevitable for improving the quality of the approximation. Nevertheless, a reduction of ϑ is also necessary to obtain reliable results, as the comparison of $((DQ), \vartheta = 0.5)$ and $((DQ), \vartheta = 1.0)$ shows. While the first approach provides already a good approximation of the droplet position using $\tau = 1.0 \cdot 10^{-4}$, the results obtained with the second one are still unsatisfactory.

4.2 Droplet movement and contact angles

In the remaining subsections, we present simulations serving as a qualitative validation of the presented discrete scheme. In this subsection, we present a simulation of a two-dimensional charged droplet which is influenced by an external electrode. Thereby, we focus on the contact angles of the droplet and the confinement of the dissolved ions to the droplet.
Given the fluidic domain $\Omega := (-5, 5) \times (0.625, 5)$, we place a semicircular shaped droplet with radius 1 and midpoint $(1, 0.625)$ on the lower boundary of Ω. The

Fig. 2 Initial triangulation

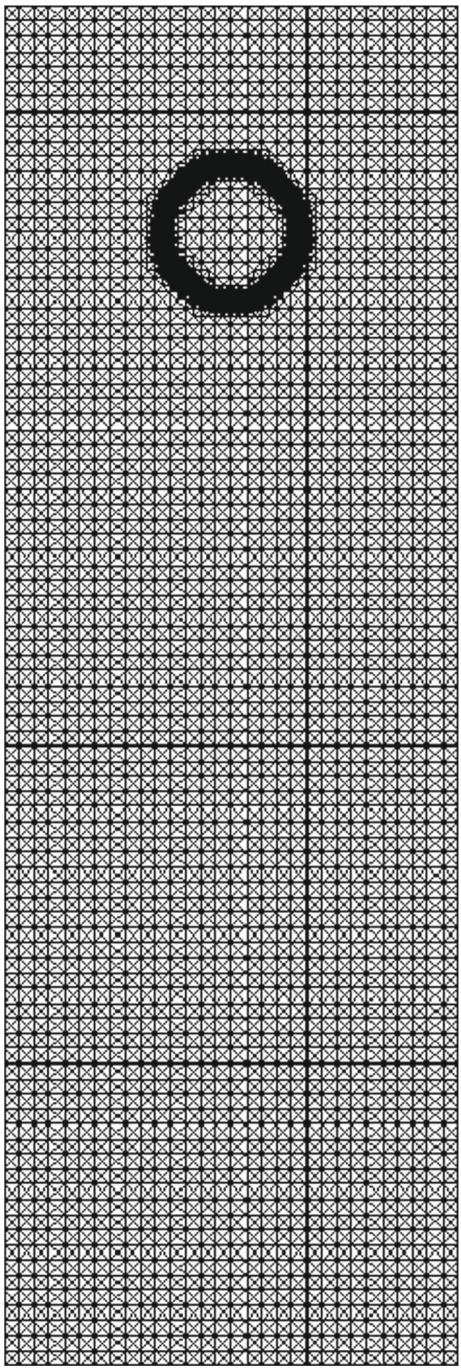

Table 1 Parameters used in Section 4.1

δ	σ	m	$\gamma_{fs}(\pm 1)$	α	$\rho(+1)$	$\rho(-1)$	$\eta(\pm 1)$
0.01	10	10^{-4}	0	0	3	1	0.05

droplet has the same density and viscosity as the ambient liquid (cf. Table 2). The choice $\sigma = 3$ allows for deformation of the droplet while still preventing breakup. The width of the fluid-fluid interface is given by $\delta = 0.02$. The stationary contact angle between interface and wall is prescribed by $\gamma_{fs} \equiv 0$ which corresponds to a contact angle of 90°. By setting $\alpha = 0.0002$, we allow the dynamic contact angles to deviate from the stationary ones. The droplet contains positively charged ions. On a semicircle with radius 0.5 and midpoint $(1, 0.625)$ we prescribe $\omega_h^0 = 10$. To avoid jumps in the initial ion concentration (indicated in gray in Fig. 6a), the number density decays linearly until it vanishes on a sphere with radius 0.75 around the midpoint $(1, 0.625)$. The ions are supposed to be soluble only in the droplet, which is achieved by setting $\beta = 1$ inside of the droplet and $\beta = 10$ in the ambient fluid (and interpolating in the interfacial region using an appropriate sin-function). The diffusivity of the ions is given by $k \equiv 5$.

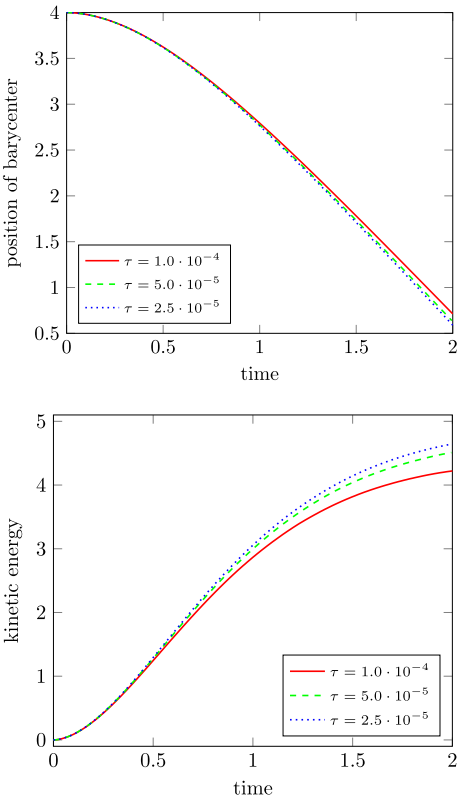

Fig. 3 Position of the droplet's barycenter and kinetic energy; computed using (DQ), $\vartheta = 0.5$

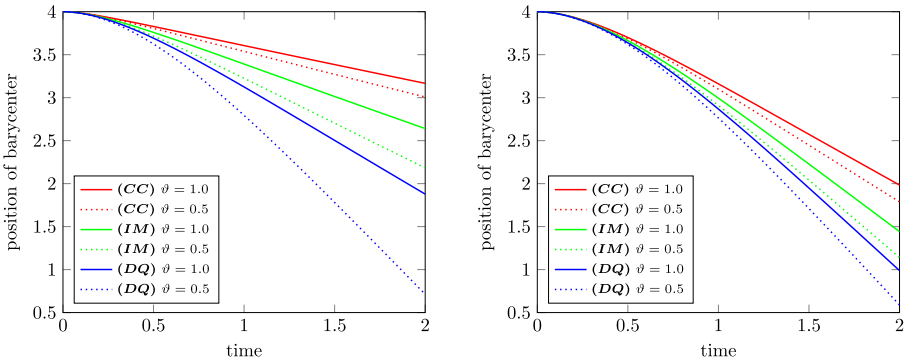

Fig. 4 Position of the droplet's barycenter computed using $\tau = 1.0 \cdot 10^{-4}$ (left) and $\tau = 2.5 \cdot 10^{-5}$ (right)

To manipulate the droplet, we place electrodes below it, i.e., we consider $\Omega^* := (-5, 5) \times (0, 10)$ and assume Dirichlet conditions on $\Gamma_b := [-5, 5] \times \{0\}$ and $\Gamma_t := [-5, 5] \times \{10\}$. While imposing homogeneous Dirichlet data on Γ_t and on most parts of Γ_b, the electrode is represented by $\overline{V} = -20$. Initially, it is placed right below the droplet, i.e. ,$\overline{V} = -20$ on $[0.5, 1.5] \times \{0\}$. Later (at $t = 0.001$) this electrode is shifted to $[-1.5, -0.5] \times \{0\}$ before returning to its original position at $t = 0.03$. On the left and right boundary of Ω^*, we impose homogeneous Neumann conditions.

The discretization parameters are chosen as follows. We use an adaptive mesh consisting of simplices with diameters between approximately 0.110 and 0.014. The fixed time increment is set to $\tau = 5 \cdot 10^{-6}$. The polynomial double-well potential is extended by a penalty term with $\delta' = 4 \cdot 10^{-3}$ (cf. (4.3)). The derivatives of the double-well potential are discretized using (DQ). Choosing $\vartheta = 0.625$, we expect the Cahn-Hilliard type equations to introduce only little numerical dissipation. For the remaining parameters, we refer to Table 2.

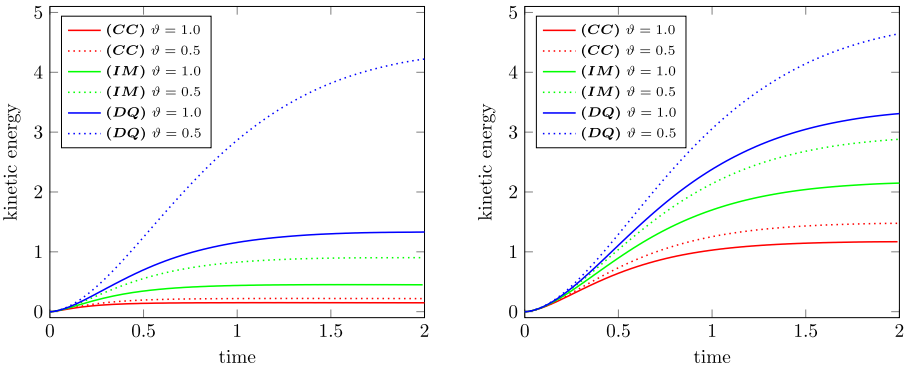

Fig. 5 Kinetic energy computed using $\tau = 1.0 \cdot 10^{-4}$ (left) and $\tau = 2.5 \cdot 10^{-5}$ (right)

Table 2 Parameters used in the simulation in Section 4.2.

σ	δ	m	$\gamma_{fs}(\pm 1)$	α	ϑ	$\rho(\pm 1)$	$\eta(\pm 1)$	ϵ	ν	τ
3	0.02	0.1	0	$2 \cdot 10^{-4}$	0.625	10^{-4}	$5 \cdot 10^{-4}$	1	10^{-7}	$5 \cdot 10^{-6}$

The position of the droplet and the distribution of the ions are depicted in Fig. 6. The black rectangle represents the fluidic domain Ω. The position of the droplet is indicated by a black curve representing the equipotential line $\phi = 0$, while the position of the electrode is marked by the thick black line below Ω. The gray shading in the background indicates the spatial distribution of the ions.

Fig. 6 Ion-induced droplet movement

Initially, the ions are placed right above the electrode. After shifting the electrode to the left, the ions try to follow the electrode carrying a portion of droplet with them (see Fig. 6a–d). As the surface tension is high enough to prevent rupture, the entire droplet moves to the left and attains a nearly semicircular shape above the new position of the electrode.

At time $t = 0.03$, the electrode is shifted back to its former position (see Fig. 6e). Consequently, the ions—and therefore the entire droplet—also move back to the right-hand side of the domain (cf. Fig. 6f–h), where the droplet finally attains a semicircular shape above the electrode.

We want to highlight two details occuring in this simulation. First, we want to point out the contact angle hysteresis at the bottom of Ω. While the droplet is moving, the contact angles of the droplet deviate significantly from the stationary one which was prescribed as $\frac{\pi}{2}$ (cf. Fig. 6c–d and f–g). In the stationary state (see Fig. 6h), the stationary contact angle of $\frac{\pi}{2}$ is recovered, as the droplet is at rest. Secondly, we want to recall that we used only an energetic argument to confine the ions to the droplet. As this simulations shows, the energetic penalization suffices to prevent the ions from leaving the droplet, although they are subjected to relatively strong forces.

4.3 Ion-induced droplet deformation

In this subsection, we consider several kinds of species and focus on topological changes like droplet breakup or droplet coalescence.

In the first scenario, we position a circular droplet ($\phi = 1$) with radius 0.3 and barycenter at $(0, 0, 0)$ in a cylindrical domain $\Omega := \{x \in \mathbb{R}^3 : -1.75 < x_1 < 1.75,\ x_2^2 + x_3^2 < 1\}$. In this simulation three different types of species are included. On the right-hand side of Fig. 7, the uncharged molecules, negatively charged ions, and positively charged ions are indicated in green, blue, and red, respectively. All three considered species types are assumed to be soluble only in the droplet, which is achieved by choosing $\beta_i(1) = 1$ (droplet), $\beta_i(-1) = 10$ (ambient liquid), and using an appropriate sin-function to interpolate between those values in the interfacial region ($i = 1, 2, 3$). The properties of the species types are specified in Table 3. The droplet initially contains only uncharged molecules, i.e., $\omega_{1,h}^0 = 2$ in an origin centered ball with radius 0.1 and decays linearly until it vanishes on the origin centered sphere with radius 0.29, while $\omega_{2,h}^0 \equiv \omega_{3,h}^0 \equiv 0$. The uncharged molecules may decompose into charged ions. The rate of decomposition and recombination is prescribed by the coefficients $\zeta_1 = -2$, $\zeta_2 = \zeta_3 = 2$ (cf. Table 3).

The electrostatic potential V is computed on $\Omega^* := \{x \in \mathbb{R}^3 : -2 < x_1 < 2,\ x_2^2 + x_3^2 < 1\}$. The base surfaces of this cylinder are assumed to be electrodes, i.e., we prescribe inhomogeneous Dirichlet data $\overline{V} = 5$ on $\{x \in \partial\Omega^* : x_1 = -2\}$ and $\overline{V} = -5$ on $\{x \in \partial\Omega^* : x_1 = 2\}$. Matching to the representation of the ion number densities, the electrodes in Fig. 7 are colored in red (positive) and blue (negative). On the lateral area of Ω^*, we impose $\nabla V \cdot n = 0$.

In this simulation, we use a penalized polynomial double-well potential (see (4.3)) with a penalty parameter $\delta' = 4 \cdot 10^{-3}$. Its derivatives are approximated using (DQ). For the remaining parameters, we refer to Table 4.

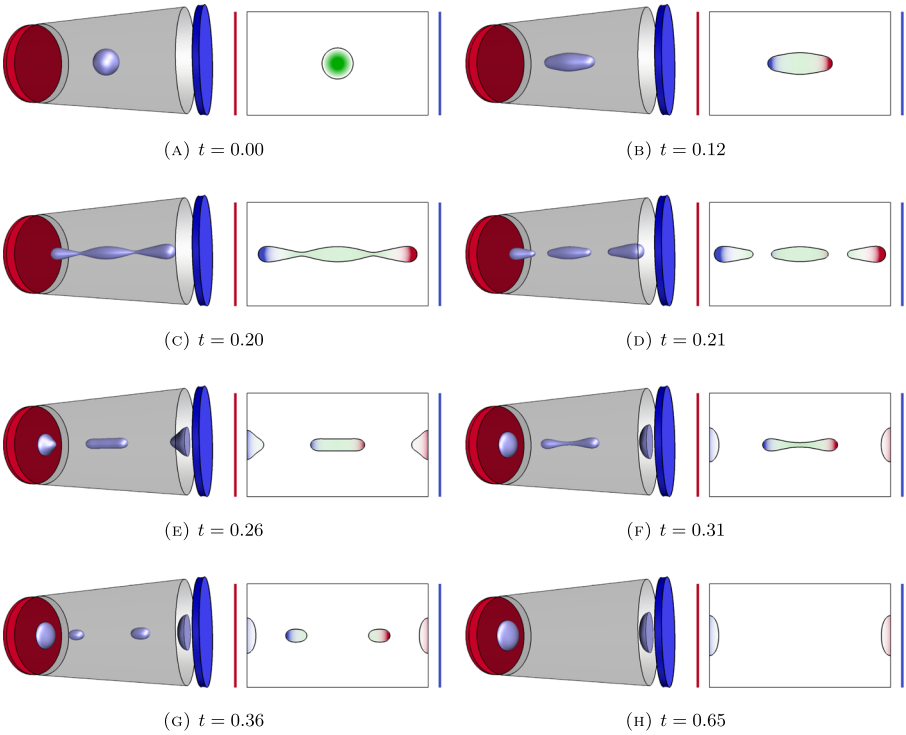

Fig. 7 Ion-induced droplet breakup. Left: droplet shape. Right: cross-section showing species distributions

Assuming rotational symmetry, we may describe the setting using cylindrical coordinates and use a two-dimensional, adaptive mesh consisting of simplices with diameters between 0.0625 and approximately 0.0055. The simulation was performed using a fixed time increment $\tau = 10^{-4}$.

Figure 7 shows the evolution of the droplet and the dissolved species. The evolution of the three-dimensional droplet is depicted on the left-hand side. The right-hand side of Fig. 7 shows a cross-section of Ω^*.

As depicted in Fig. 7b, the molecules start decomposing into ions which move towards the electrodes. As the species are only soluble in the droplet, this movement causes the droplet to stretch—resulting in neckings (see Fig. 7c) and finally in the

Table 3 Species parameters used in the simulation in Section 4.3

species	z_i	$k_i(\pm 1)$	ζ_i	$\beta_i(-1)$	$\beta_i(+1)$
$i = 1$	0	2	-2	10	1
$i = 2$	-3	2	2	10	1
$i = 3$	3	2	2	10	1

Table 4 Parameters used in the simulation in Section 4.3

σ	δ	m	$\gamma_{fs}(\pm 1)$	α	ϑ	$\rho(\pm 1)$	$\eta(\pm 1)$	ϵ	ν	τ
0.1	0.01	0.05	0	0	1	10^{-4}	0.05	0.5	10^{-5}	10^{-4}

breakup of the droplet (see Fig. 7d). As most of the ions are located in the detached satellite droplets, the central droplet, which still contains uncharged molecules, is hardly affected by the electric field for a short period of time and therefore tries to recover a circular shape. At the same time, the satellite droplets continue drifting towards the electrodes. Since the decomposition of the molecules continues, the ion concentration in the central droplet rises again—resulting once again in stretching, necking and rupture of the droplet (see Fig. 7e–g). At the end of the simulation (see Fig. 7h), there are two charged droplets positioned at the base surfaces of Ω. Although the droplets try to minimize their surface, they do not attain a hemispherical shape, as they also try to maximize the contact area with $\partial\Omega$ in order to allow the ions to get as close to the electrodes as possible without piling up.

In the first scenario, the influence of the ions on the electrostatic potential was negligible in comparison to the influence of the prescribed boundary data. In the second scenario, we reduce the impact of the boundary conditions by choosing grounded electrodes which are placed further away from the fluidic domain, i.e., we choose $\Omega^* := \{x \in \mathbb{R}^3 : -3 < x_1 < 3,\ x_2^2 + x_3^2 < 1\}$ with homogeneous Dirichlet conditions on the base surfaces. Again, on the lateral area $\nabla V \cdot n = 0$ is imposed. We position circular droplets with radius 0.3 and barycenters at $(\pm 0.5, 0, 0)$. Initially, these droplets contain ions. Similarly to the last scenario, we prescribe $\omega_{2,h}^0 = 2$ and $\omega_{3,h}^0 = 2$ in a ball with radius 0.1 and assume linear decay until the number density vanishes on a sphere with radius 0.29 (see Fig. 7a). The positively charged ions are placed in the left droplet, i.e., the barycenter of their number density is at $(-0.5, 0, 0)$, and the negatively charged ions are placed around $(0.5, 0, 0)$. The initial number density of the uncharged molecules is set to zero. The remaining parameters stay unchanged and can be found in Tables 3 and 4. Again, the derivatives of the penalized, polynomial double-well potential with $\delta' = 4 \cdot 10^{-3}$ are approximated using (DQ).

Figure 8 shows the evolution of the droplet and the dissolved species. Thereby, some figures show the three-dimensional droplets, while others show a cross-section. The grounded electrodes which are placed farther from the fluidic domain are not depicted. The color of the droplets in Fig. 8a, d, and h indicates the electrostatic potential on the zero level line of the phase-field (red: positive; blue: negative; green: ≈ 0). In the figures depicting the cross-section, the colors indicate the number densities of the species ($\omega_{1,h}$: green; $\omega_{2,h}$: blue; $\omega_{3,h}$: red). The arrows visualize the electric field, i.e. $-\nabla V$. The grounded electrodes are placed outside of the picture. As depicted in Fig. 8, the droplets move towards each other, collide, and finally merge. As soon as the droplets merge, the electrical charges equilibrate causing the disappearance of the electric field (see Fig. 8f–g). At the same time the reaction starts and

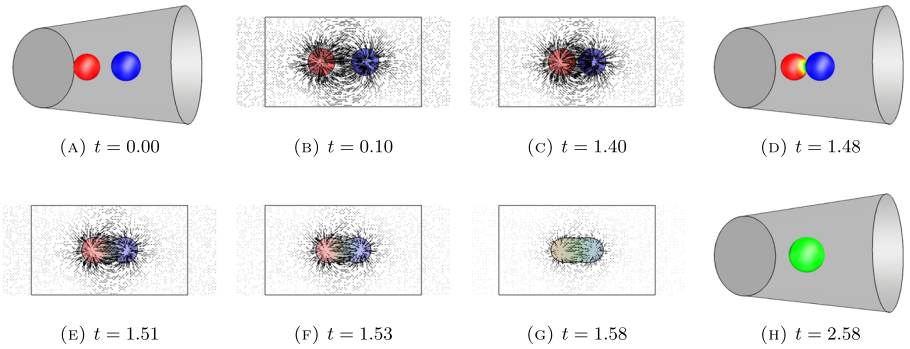

Fig. 8 Ion-induced droplet coalescence

produces uncharged molecules. After some time only one uncharged, circular shaped droplet remains (see Fig. 8h). This droplet still contains a significant amount of ions, but as the ion charges cancel out each other, the entire droplet is uncharged.

Funding information This research has been supported by Deutsche Forschungsgemeinschaft (German Science Foundation) through the Priority Programme 1506 "Transport processes at fluidic interfaces".

References

1. Abels, H., Garcke, H., Grün, G.: Thermodynamically consistent, frame indifferent diffuse interface models for incompressible two-phase flows with different densities. Math. Model. Methods Appl. Sci. **22**(3), 1150013 (2012)
2. Aland, S., Boden, S., Hahn, A., Klingbeil, F., Weismann, M., Weller, S.: Quantitative comparison of Taylor flow simulations based on sharp-interface and diffuse-interface models. Int. J. Numer. Methods Fluids **73**(4), 344–361 (2013)
3. Armero, F., Simo, J.C.: Formulation of a new class of fractional-step methods for the incompressible MHD equations that retains the long-term dissipativity of the continuum dynamical system. Fields Inst Commun **10**, 1–24 (1996)
4. Brenner, S.C., Scott, L.R.: The mathematical theory of finite element methods. Springer, Berlin (2002)
5. Campillo-Funollet, E., Grün, G., Klingbeil, F.: On modeling and simulation of electrokinetic phenomena in two-phase flow with general mass densities. SIAM J. Appl. Math. **72**(6), 1899–1925 (2012). https://doi.org/10.1137/120861333
6. Ciarlet, Ph.G.: The finite element method for elliptic problems. North-Holland, Amsterdam (1978)
7. Copetti, M.I.M., Elliott, C.M.: Numerical analysis of the Cahn–Hilliard equation with a logarithmic free Energy. Numer. Math. **63**, 39–65 (1992)
8. Eck, C., Fontelos, M.A., Grün, G., Klingbeil, F., Vantzos, O.: On a phase-field model for electrowetting. Interfaces Free Boundaries **11**, 259–290 (2009)
9. Fontelos, M.A., Grün, G., Jörres, S.: On a phase-field model for electrowetting and other electrokinetic phenomena. SIAM J. Math. Anal. **43**(1), 527–563 (2011)
10. Grün, G.: Partiell gleichmäßige Konvergenz finiter Elemente bei quasikonvexen Variationsintegralen. Diploma Thesis (Universität Bonn), Bonn (1991)
11. Grün, G.: On convergent schemes for diffuse interface models for two-phase flow of incompressible fluids with general mass densities. SIAM J. Numer. Anal. **6**, 3036–3061 (2013)
12. Grün, G., Guillén-González, F., Metzger, S.: On fully decoupled, convergent schemes for diffuse interface models for two-phase flow with general mass densities. Commun. Comput. Phys. **19**(5), 1473–1502 (2016). https://doi.org/10.4208/cicp.scpde14.39s

13. Grün, G., Klingbeil, F.: Two-phase flow with mass density contrast: stable schemes for a thermodynamic consistent and frame-indifferent diffuse-interface model. J. Comput. Phys. **257, Part A**, 708–725 (2014)
14. Grün, G., Rumpf, M.: Nonnegativity preserving convergent schemes for the thin film equation. Numer. Math. **87**, 113–152 (2000). MR 1800156 (2002h:76108)
15. Guillén-González, F., Tierra, G.: Splitting schemes for a Navier–Stokes–Cahn–Hilliard model for two fluids with different densities. J. Comput. Math. **32**(6), 643–664 (2014)
16. Garcke, C., Kahle, H., Hinze, M.: A stable and linear time discretization for a thermodynamically consistent model for two-phase incompressible flow. Hamburger beiträge zur Angewandte Mathematik (2014)
17. Klingbeil, F.: On the numerics of diffuse-interface models for two-phase flow with species transport. Ph.D. thesis, friedrich-alexander-universität erlangen-nürnberg, Erlangen (2014)
18. Metzger, S.: On numerical schemes for phase-field models for electrowetting with electrolyte solutions. PAMM **15**(1), 715–718 (2015). https://doi.org/10.1002/pamm.201510346
19. Metzger, S.: Diffuse interface models for complex flow scenarios: modeling, analysis and simulations. Ph.D. thesis, Friedrich-Alexander-Universität Erlangen-Nürnberg, Erlangen (2017)
20. Minjeaud, S.: An unconditionally stable uncoupled scheme for a triphasic Cahn–Hilliard/Navier-Stokes model. Num. Methods PDE **29**(2), 584–618 (2013)
21. Nochetto, R.H., Salgado, A.J., Walker, S.W.: A diffuse interface model for electrowetting with moving contact lines. Math. Model Methods Appl. Sci. **24**(1), 67–111 (2014)
22. Qian, T., Wang, X., Sheng, P.: A variational approach to the moving contact line hydrodynamics. J. Fluid Mech. **564**, 333–360 (2006)
23. Werner, H., Arndt, H.: Gewöhnliche Differentialgleichungen. Springer, Berlin–Heidelberg (1991)